





The mitochondrial ribosomal protein mRpL4 regulates Notch signaling

Dongqing Mo^{1,†}, Chenglin Liu^{2,3,4,†} , Yao Chen¹, Xinkai Cheng^{2,3,4}, Jie Shen¹ , Long Zhao^{2,3,4}  & Junzheng Zhang^{1,*} 

Abstract

Mitochondrial ribosomal proteins (MRPs) assemble as specialized ribosome to synthesize mtDNA-encoded proteins, which are essential for mitochondrial bioenergetic and metabolic processes. MRPs are required for fundamental cellular activities during animal development, but their roles beyond mitochondrial protein translation are poorly understood. Here, we report a conserved role of the mitochondrial ribosomal protein L4 (mRpL4) in Notch signaling. Genetic analyses demonstrate that mRpL4 is required in the Notch signal-receiving cells to permit target gene transcription during *Drosophila* wing development. We find that mRpL4 physically and genetically interacts with the WD40 repeat protein wap and activates the transcription of Notch signaling targets. We show that human mRpL4 is capable of replacing fly mRpL4 during wing development. Furthermore, knockout of *mRpL4* in zebrafish leads to downregulated expression of Notch signaling components. Thus, we have discovered a previously unknown function of mRpL4 during animal development.

Keywords *Drosophila*; mitochondrial ribosomal protein L4; Notch; wap; zebrafish

Subject Categories Development; Metabolism; Signal Transduction

DOI 10.15252/embr.202255764 | Received 10 July 2022 | Revised 7 March 2023 | Accepted 18 March 2023 | Published online 3 April 2023

EMBO Reports (2023) 24: e55764

Introduction

Mitochondria are best known as the powerhouse of cells as they generate the majority of cellular ATP through coupled reactions carried out by five oxidative phosphorylation (OXPHOS) protein complexes (Quirós *et al.*, 2016). Most OXPHOS proteins are generated from nuclear genes and imported into mitochondria, with the exception of 13 OXPHOS proteins encoded by the mitochondrial genome (Richter-Dennerlein *et al.*, 2015). The mitochondrial protein

synthesis depends on the mitochondrial ribosomal proteins (MRPs), which assemble to form a specialized form of ribosome (Kummer & Ban, 2021). Disruption of MRPs function leads to deficiency in OXPHOS protein synthesis and mitochondrial activity, which in turn impacts a wide variety of cellular processes (Kummer & Ban, 2021).

Systemic mutagenesis analysis in *Drosophila* (Marygold *et al.*, 2007) and mice (Cheong *et al.*, 2020) have demonstrated that MRPs are crucial for animal development. Mutations of MRPs are associated with a number of developmental disorders and fatal diseases in humans (Huang *et al.*, 2020; Ferrari *et al.*, 2021). The impacts of MRPs on fundamental developmental events such as cell cycle and cell growth have been extensively investigated (Galloni, 2003; Frei *et al.*, 2005; Mandal *et al.*, 2005; Tselykh *et al.*, 2005; Liao *et al.*, 2006; Ohsawa *et al.*, 2012; Wang *et al.*, 2012; Chen *et al.*, 2018a). These findings highlight the importance of MRPs for mitochondrial activity and fit well with current view that mitochondria function not only as the power generator but also as a signaling hub (Quirós *et al.*, 2016). Recent studies have begun to reveal the diversified roles of MRPs, some of which are independent of mitochondrial protein synthesis (Amikura *et al.*, 2001; Zhang *et al.*, 2015; Han *et al.*, 2020; Huang *et al.*, 2020). However, the functions of MRPs outside of mitochondrial ribosome during animal development are not fully understood.

The highly conserved Notch signaling pathway functions to distinguish adjacent cells and is required for various developmental processes (Bray, 2006). In *Drosophila*, the *Notch* gene encodes a transmembrane receptor, which is activated by Delta or Serrate presented on the membrane of signal-sending cell (Henrique & Schweisguth, 2019). The receptor–ligand engagement triggers a series of proteolytic cleavage of the Notch protein and releases the Notch intracellular domain (NICD). NICD is translocated into the nucleus, where it forms a transcription activation complex with the DNA-binding protein Suppressor of Hairless [Su(H)] to drive the expression of downstream target genes (Guruharsha *et al.*, 2012). In the absence of Notch activation, Su(H) recruits co-repressors to suppress the expression of Notch targets (Henrique & Schweisguth, 2019).

1 Department of Plant Biosecurity and MOA Key Laboratory of Surveillance and Management for Plant Quarantine Pests, College of Plant Protection, China Agricultural University, Beijing, China

2 Institute of Evolution & Marine Biodiversity, Ocean University of China, Qingdao, China

3 College of Fisheries, Ocean University of China, Qingdao, China

4 Key Laboratory of Mariculture (OUC), Ministry of Education, Qingdao, China

*Corresponding author. Tel: +86 10 62733762; E-mail: zhangjz@cau.edu.cn

†These authors contributed equally to this work

The Notch signaling cascade regulates mitochondrial homeostasis and activity in both fly and vertebrates (Thörig *et al.*, 1981a,b; Vilkki & Portin, 1987; Landor *et al.*, 2011; Basak *et al.*, 2014; Ludikhuize *et al.*, 2020; Dubal *et al.*, 2022), but only a few mitochondrial proteins are directly regulated by Notch signaling at the transcriptional level (Xu *et al.*, 2015; Lee & Long, 2018; Kung-Chun Chiu *et al.*, 2019). Interestingly, NICD also functions through Su(H)-independent pathways to regulate mitochondria activity (Perumalsamy *et al.*, 2010; Xu *et al.*, 2015; Chen *et al.*, 2018b; Zhou *et al.*, 2019; Dai *et al.*, 2020). In this noncanonical pathway, NICD is found to localize in the mitochondria and interact with various mitochondrial proteins, including the OXPHOS components (Lee *et al.*, 2013; Ojha *et al.*, 2022). The cross talk between mitochondria and Notch signaling is bidirectional, with studies in *Drosophila* follicle cells showing for the first time that mitochondria fission activates Notch signaling (Mitra *et al.*, 2012). Subsequent studies reveal that mitochondria modulate Notch activity through signaling molecules such as calcium (Kasahara *et al.*, 2013) and reactive oxygen species (ROS; Hamanaka *et al.*, 2013; Cao *et al.*, 2016; Khacho *et al.*, 2016; Perez-Gomez *et al.*, 2020). However, our understanding about the reciprocal regulatory relationship between mitochondria and Notch signaling is still incomplete.

We have isolated an MRP gene, *mRpl4*, as a positive regulator of Notch signaling during *Drosophila* wing development. We found that mRpl4 functions in the Notch signal-receiving cells to permit transcription of target genes. Likely independent of its role in OXPHOS protein synthesis, mRpl4 interacts with wap to facilitate the recruitment of Su(H) to the chromatin. We further demonstrate that knockout of mRpl4 in zebrafish leads to decreased Notch signaling activity. Our findings reveal a previously unknown function of MRP during animal development and emphasize the complexity of Notch signaling regulation.

Results

mRpl4 regulates Notch signaling activity in the *Drosophila* wing

During a somatic mosaic screen (Mo *et al.*, 2022), one of the Bruinfly mutant stocks, *mRpl4*^{K14608}, was found to cause marginal defects when homozygous clones were generated in the wings (Fig 1A). As this phenotype is reminiscent of impaired Notch signaling, we examined the expression level of Notch target genes *Cut* and *Wingless* (*Wg*). In the wild-type wing imaginal disk, *Cut* (Appendix Fig S1A) and *Wg* (Appendix Fig S1B) were produced in cells located at the dorsal/ventral (D/V) boundary. In *mRpl4*^{K14608} homozygous clones located at the D/V boundary, the expression of *Cut* and *Wg* was abolished (Fig 1B and C). The expression of Notch activity reporter *NRE-GFP* (Saj *et al.*, 2010) was also reduced in *mRpl4*^{K14608} mutant cells (Fig 1D). The expression of Notch (Appendix Fig S1C and D) and *Dl* (Appendix Fig S1E and F) was not significantly affected in *mRpl4* mutant cells. Importantly, when a *mRpl4* transgene was expressed in *mRpl4*^{K14608} mutant cells using the MARCM technique (Lee & Luo, 2001), the Notch signaling defect was rescued (Fig 1E and F; Appendix Fig S1G and H).

Consistent with the mutant phenotypes, inhibiting the expression of *mRpl4* by RNAi also led to marginal nicks in the adult wing (Fig 2A). The *mRpl4* RNAi resulted in moderate wing margin

defects, while RNAi knockdown of two other MRP genes (*mRps28* and *mRpl24*) showed little effect on wing margin integrity (Appendix Fig S2A–D). The *mRpl4* transgene was sufficient to rescue both the adult wing margin defect (Fig 2A) and downregulation of *Cut* in the wing disk (Fig 2B) when co-expressed with the RNAi construct. When *mRpl4* RNAi was driven by *hh-Gal4* in the posterior compartment of wing disk, the expression of *Cut* and *Wg* was clearly dampened within the posterior region (Fig 2C; Appendix Fig S2E).

Notch signaling plays important roles during the development of numerous tissues, and whether mRpl4 is broadly involved in the regulation of Notch signaling was further investigated. Notch signal activity could be readily monitored by reporter lines such as *NRE-GFP* in larval neuroblasts (Liu *et al.*, 2017) and salivary gland imaginal rings (Yang & Deng, 2018), as well as by *Su(H)-LacZ* in adult midgut (Zhao *et al.*, 2022). RNAi knockdown of *mRpl4* but not *mRpl24* was able to attenuate the expression of *NRE-GFP* in larval neuroblasts (Fig EV1A–C) and salivary gland imaginal rings (Fig EV1D–F). In adult midgut, the expression level of *Su(H)-LacZ* was also reduced by *mRpl4* RNAi (Fig EV1G–I). These observations indicate that mRpl4 might modulate Notch signaling in various developmental events.

Activation of Notch signaling relies on binding of Su(H) at the enhancer region of target genes (Krejci & Bray, 2007; Gomez-Lamarca *et al.*, 2018). When examined by chromatin immunoprecipitation (ChIP) in wing disk cells, mRpl4 knockdown by RNAi was found to decrease the occupancy of Su(H) at regulatory regions of the *Enhancer of split Complex* family genes (Fig 2D), as well as at enhancer regions of *Cut*, *Wg*, and *Vestigial* (Fig EV1J). Collectively, these findings demonstrate that mRpl4 positively regulates Notch signaling activity.

mRpl4 functions in signal-receiving cells

Previous studies have shown that *mRpl4* is involved in fly eye and ovary development (Mandal *et al.*, 2005; Ohsawa *et al.*, 2012; Wang *et al.*, 2012), but its role in Notch signaling has not been reported. Therefore, we performed genetic analysis to further dissect the role of mRpl4 in Notch signal transduction. To distinguish whether mRpl4 functions in the signal-sending or receiving cells, the MARCM system was employed to overexpress *Dl*, *Ser*, and Notch proteins in *mRpl4*^{K14608} mutant cells. Expression of *Dl* in wild-type cells led to the induction of *Wg* expression along the border of MARCM clones (Fig EV2A). Overexpression of *Dl* in *mRpl4*^{K14608} clones also induced *Wg* expression in the surrounding cells (Fig EV2B). Similarly, overexpression of *Ser* led to the induction of *Wg* along the border of MARCM clones in both wild-type (Fig EV2C) and *mRpl4*^{K14608} mutant (Fig EV2D) cells. These results suggest that mRpl4 is dispensable in the signal-sending cells.

Similar experiment with full-length Notch (*N^{FL}*) was performed to investigate the role of mRpl4 in the signal-receiving cells. In wild-type cells, *N^{FL}* induced *Cut* expression in proximity of the wing margin (Fig 3A). However, *N^{FL}* failed to induce *Cut* expression in *mRpl4*^{K14608} clones (Fig 3B). These observations indicate a requirement for mRpl4 in the signal-receiving cells to activate Notch targets.

In the signal-receiving cells, an active membrane-bound form of Notch (NEXT) is generated through proteolytic cleavage by the metalloprotease Kuzbanian after binding with the ligands. NEXT is

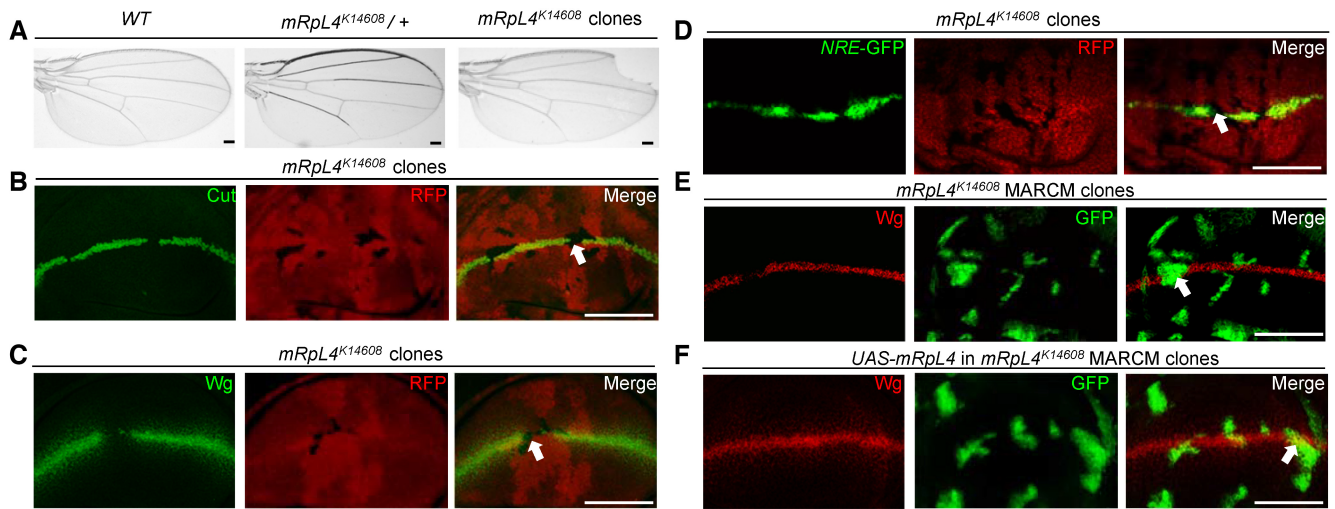


Figure 1. mRpl4 mutant leads to Notch signaling defects in the *Drosophila* wing.

A Representative image of wings ($n > 20$ wings) from control adult flies, $mRpl4^{K14608}$ heterozygous flies and flies harboring $mRpl4^{K14608}$ homozygous mutant clones.
 B–D Representative image of wing imaginal disks ($n > 15$ wing disks) stained for Cut and Wg, and wing disk expressing Notch signaling reporter *NRE-GFP*, respectively.
 E, F Representative images of wing disks ($n > 10$ wing disks) bearing MARCM clones stained for Wg. In (F), *UAS-mRpl4* are expressed under the control of *tub-Gal4* in the MARCM clones.

Data information: The $mRpl4^{K14608}$ mutant clones in these images are marked by the absence of RFP (B–D), while the MARCM clones are marked by GFP (E, F). Representative clones are marked by white arrows in (B–F). Scale bars = 100 μ m.

further cleaved by Presenilin to form NICD, which interacts with Su (H) to regulate target gene expression (Bray, 2006). To refine in which step mRpl4 is required for Notch processing, we overexpressed NEXT and NICD in $mRpl4^{K14608}$ mutant cells. In wild-type cells, NEXT was sufficient to induce the expression of downstream target Cut (Fig 3C). NEXT failed to induce the expression of Cut in $mRpl4^{K14608}$ clones (Fig 3D). Furthermore, we found that NICD robustly induced Cut expression in wild-type cells (Fig 3E), but failed to do so in $mRpl4^{K14608}$ mutant cells (Fig 3F). The expression of N^{FL} (Fig EV2E), NEXT (Fig EV2F), and NICD (Fig EV2G and H) in MARCM clones was confirmed by immunostaining using antibody raised against NICD. These genetic data place the function of mRpl4 downstream of NICD production to regulate target gene expression.

mRpl4 regulates OXPHOS activity and Notch signal through parallel pathways

Mitochondrial ribosomal proteins are required for optimal mitochondrial activity, and ROS, a major metabolite of mitochondria, has been shown to modulate Notch signaling activity in various developmental contexts (Hamanaka et al, 2013; Cao et al, 2016; Khacho et al, 2016; Perez-Gomez et al, 2020). The cellular ROS level was indeed reduced in both $mRpl4^{K14608}$ mutant clones and mRpl4 RNAi cells (Fig 4A and B), implying that the effect of mRpl4 on Notch signal transduction might be relayed by ROS. However, several findings are inconsistent with this simplified model. Mutations of two other MRP genes, *mRps28* and *mRpl24*, led to reduction of ROS without affecting Cut expression (Fig 4C and D). In addition, RNAi knockdown of *mRps2* and *mRps12* impaired ROS production but not Cut expression (Fig 4E and F). We further examined the role of Cytochrome c oxidase Va (CoVa) during wing development. CoVa

is a component of the OXPHOS complex IV, which functions downstream of mRpl4 to regulate cell cycle progression (Mandal et al, 2005; Mitra et al, 2012). The production of ROS was inhibited in *CoVa^{tend}* mutant clones (Fig 4G) and CoVa RNAi cells (Figs 4H and EV3A), but Cut was expressed normally (Figs 4G and H and EV3B). Unlike *CoVa* and *mRpl4* mutations, inhibition of other OXPHOS complexes led to accumulation of ROS (Fig EV3C–F), which could induce oxidative stress response and trigger changes in multiple signaling pathways (Owusu-Ansah et al, 2008; Ohsawa et al, 2012; Wang et al, 2012; Perez-Gomez et al, 2020). Taken together, we conclude that reduction of cellular ROS is not the cause of Notch signaling defects during fly wing development. We hypothesize that additional factors are involved in the regulation of Notch signal transduction by mRpl4.

mRpl4 interacts with wap to regulate Notch signaling

In order to understand how mRpl4 regulates Notch pathway, we screened for mRpl4 interacting proteins by yeast two-hybridization and found that wings apart (*wap*, also known as Riquiqui) and mRpl50 physically interact with mRpl4 (Fig EV3G). The interaction between mRpl4 and mRpl50 fits with the fact that they are both components of the large subunit of mitochondrial ribosome. As a WD40-repeat protein, *wap* regulates Hippo and extracellular signal-regulated kinase (ERK) pathways during fly wing development (Degoutin et al, 2013; Yang et al, 2016), but its interaction with MRPs and Notch signaling has not been reported. To confirm that *wap* is an mRpl4-interacting protein, we performed immunoprecipitation experiments with wing disk cell lysates. Using an antibody developed against fly mRpl4 protein (Fig 5A), a physical association between *wap* and mRpl4 was

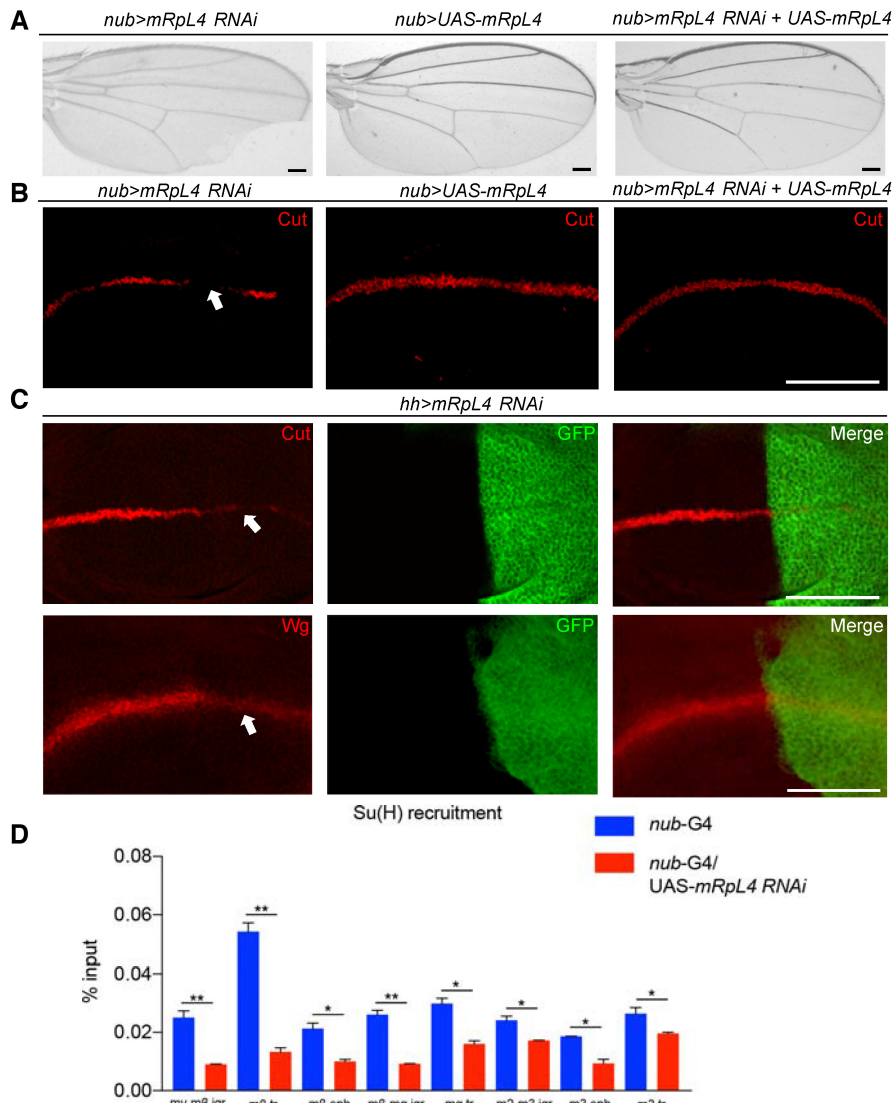


Figure 2. mRpL4 regulates Notch signaling in the *Drosophila* wing.

A Representative image of wings ($n > 20$ wings) from flies expressing *mRpL4 RNAi*, *UAS-mRpL4* and both under the control of *nub-Gal4*.

B Representative image of wing imaginal disks ($n > 15$ wing disks) stained for Cut, from flies expressing *mRpL4 RNAi*, *UAS-mRpL4* and both under the control of *nub-Gal4*.

C Representative images of wing disks ($n > 15$ wing disks) stained for Cut and Wg from flies expressing *UAS-mRpL4-RNAi* under the control of *hh-Gal4* (marked by GFP).

D The level of Su(H) occupancy at *E(spl)mβ* gene family regions as assessed by qPCR following ChIP, from wild-type and *UAS-mRpL4-RNAi*-expressing wing disks. Data are presented as mean \pm SEM, two biological replicates for each genotype and three technical replicates for each sample. Statistical significance was tested using two-tailed unpaired *t*-test. * $P < 0.05$, ** $P < 0.01$.

Data information: Representative regions showing Notch activity defects are marked by white arrows in (B, C). Scale bars = 100 μ m.

detected (Fig 5B). The potential role of *wap* in Notch signal transduction was further investigated. RNAi knockdown of *wap* led to wing margin notches (Fig 5C). In the wing disk, the expression of Cut (Fig 5D) and Notch activity reporter *E(spl)mβ-LacZ* (Figs 5E and EV3H) was attenuated in *wap* RNAi cells, while ROS production was largely unaffected (Fig 5F). Similar as that for mRpL4, knockdown of *wap* showed little effect on Notch or D1 (Fig EV3I and J). Importantly, *wap* was sufficient to restore the expression of Wg in *mRpL4^{K14608}* mutant cells (Fig 5G). These results suggest

that *wap* acts as a downstream factor of mRpL4 to regulate Notch activation in the wing.

Mitochondrial ribosomal proteins are believed to function within mitochondria to synthesize OXPHOS proteins (Kummer & Ban, 2021). However, mRpL4 (Fig EV4A) and *wap* (Fig EV4B) were found in both cytoplasm and nucleus when overexpressed in fly salivary gland cells. Fractionation assays using wing disk cell lysates confirmed that endogenous mRpL4 protein was present in both the cytoplasmic and nucleus fractions (Fig EV4C). The

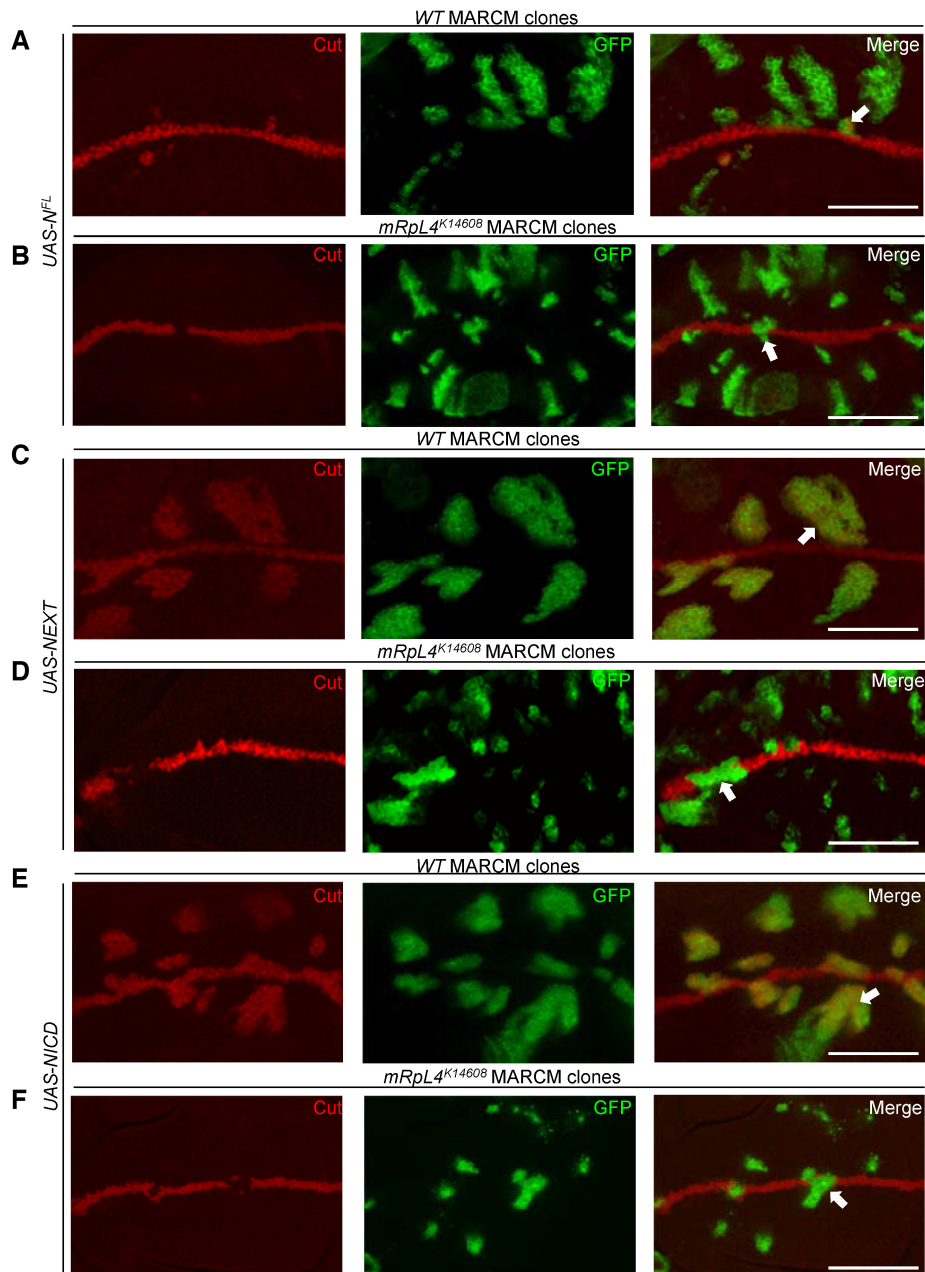


Figure 3. mRpl4 is required in Notch signal-receiving cells.

A–F Representative image of wing disks ($n > 10$ wing disks) bearing MARCM clones stained for Cut. N^{FL} (A, B), NEXT (C, D) and NICD (E, F) are overexpressed in wild-type (A, C, E) or $mRpl4^{K1460B}$ mutant (B, D, F) cells. The MARCM clones are marked by GFP and representative clones are marked by white arrows. Scale bars = 100 μ m.

presence of mRpl4 in cell nucleus is of particular interest, as we have shown that mRpl4 functions downstream of NICD to regulate Notch signal transduction. It has been reported that the Ser/Thr protein kinase minibrain (mnb) forms a heterodimer with wap, which phosphorylates key signaling components during fly wing development (Degoutin *et al*, 2013; Yang *et al*, 2016). A physical interaction between mnb and mRpl4 was detected by immunoprecipitation using wing disk cell lysates (Fig EV4D). RNAi knock-down of mnb in the developing wing resulted in wing margin

nicks (Fig 5H) and reduction of Cut expression (Fig 5I). Searching of the mnb targeting sequence (Degoutin *et al*, 2013) identified residues [T426 in Su(H) and S2659 in Notch] that could be potentially recognized and phosphorylated by the wap-mnb heterodimer (Fig EV4E and F). In wing disk cells, Su(H) was found to interact with wap when examined by immunoprecipitation (Fig EV4G). Taken together, we propose a model that mRpl4 interacts with wap-mnb to regulate Notch signaling activity, probably acting on Su(H) to modulate the transcriptional output.

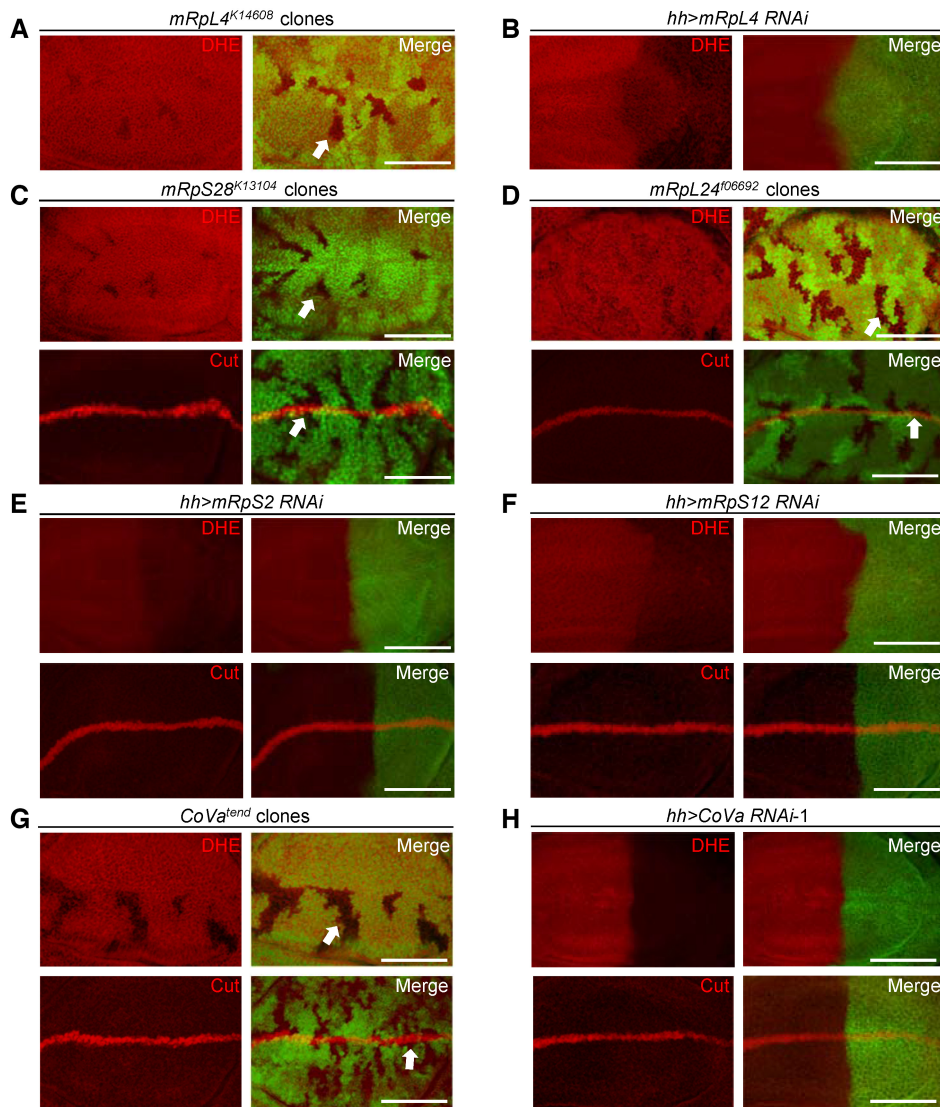


Figure 4. Subset of MRPs regulate ROS production but not Notch activity.

A, B Representative images of wing disks ($n > 15$ wing disks) stained with DHE. The $mRpL4^{K14608}$ mutant clones are marked by the absence of GFP (A), while $UAS-mRpL4-RNAi$ are expressed in the posterior region (B).
 C, D Representative images of wing disks ($n > 10$ wing disks) bearing $mRpS28^{K13104}$ (C) and $mRpL24^{f06692}$ (D) mutant clones stained with DHE and Cut.
 E, F Representative images of wing disks ($n > 15$ wing disks) stained with DHE and Cut. The $hh-Gal4$ (marked by GFP) is used to drive the expression of RNAi against $mRpS2$ (E) and $mRpS12$ (F).
 G Representative images of wing disks ($n > 10$ wing disks) bearing $CoVa^{tend}$ mutant clones stained with DHE and Cut.
 H Representative images of wing disks ($n > 15$ wing disks) stained with DHE and Cut. $UAS-CoVa-RNAi$ are expressed in the posterior region under the control of $hh-Gal4$ (marked by GFP).

Data information: The clones are marked by the absence of GFP and representative clones are marked by white arrows (A, C, D, G). Scale bars = 100 μ m.

The role of mRpL4 in Notch signaling regulation is conserved

MRPs are known to play highly conserved roles for mitochondrial protein synthesis (Richter-Dennerlein *et al.*, 2015). Our findings indicate a moonlighting role of fly mRpL4 in Notch signaling regulation, whether such additional function is a common feature across different species or specifically acquired by *Drosophila* is an intriguing question. Amino acid sequence alignment reveals that mRpL4 is highly conserved from fly to human (Fig 6A). A transgenic fly

expressing human mRpL4 protein was constructed to examine the biological activity of the homologous protein during fly wing development. The human *mRpL4* transgene was sufficient to rescue both the adult wing margin defect (Fig 6B) and downregulation of Cut in the wing disk (Fig 6C) when co-expressed with the RNAi construct. Importantly, the human mRpL4 protein was sufficient to restore both Wg expression (Fig 6D) and ROS production (Fig 6E) in $mRpL4^{K14608}$ mutant cells. These results indicate that mRpL4 might play a conserved role in Notch signal regulation.

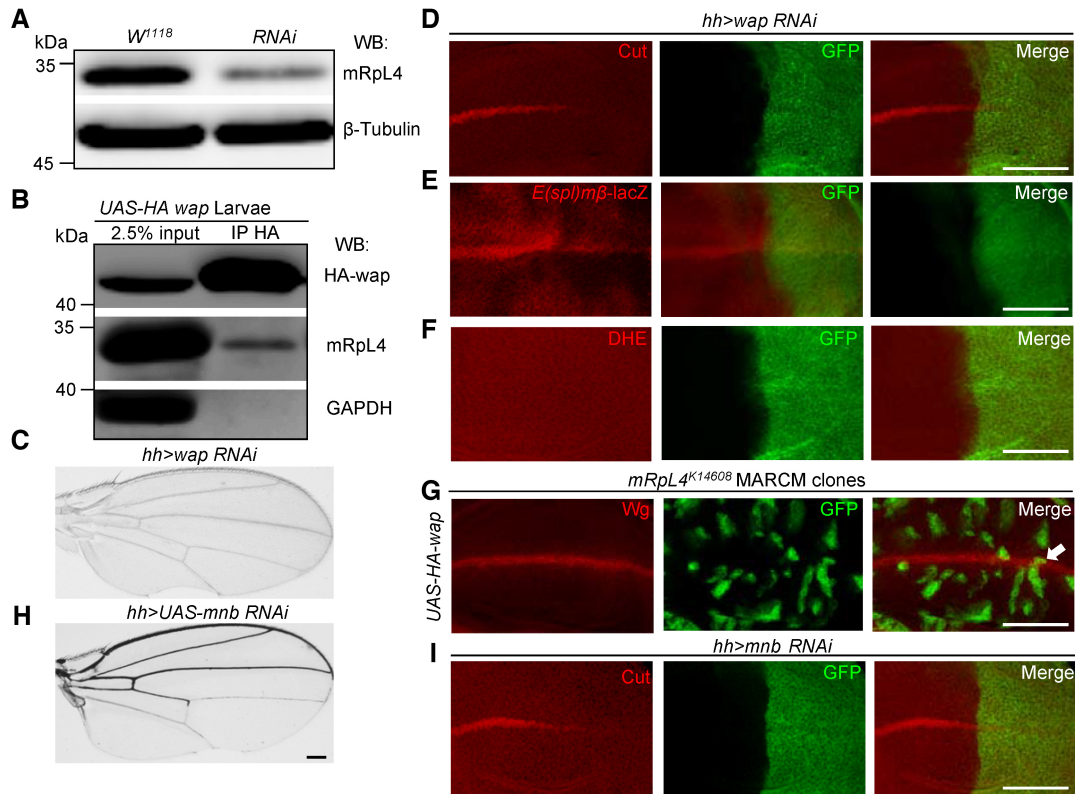


Figure 5. mRpl4 physically and genetically interacts with wap.

- A Representative western blotting ($n = 3$ biological repeats) of lysates from wild-type and *UAS-mRpl4-RNAi*-expressing wing disks. The custom mRpl4 antibody was used and the β -tubulin protein was included as loading control.
- B Representative immunoprecipitation analysis ($n = 3$ biological repeats) using lysates from wing disks overexpressing HA-tagged wap. Anti-HA antibodies were used for immunoprecipitation. Western blotting was performed using anti-HA and anti-mRpl4 antibodies to reveal wap and mRpl4, respectively. GAPDH was used as control.
- C Representative image of wings ($n > 15$ wings) from flies expressing *UAS-wap-RNAi* under the control of *hh-Gal4*.
- D–F Representative images of wing disks ($n > 15$ wing disks) from flies expressing *UAS-wap-RNAi* under the control of *hh-Gal4* that have been stained for Cut (D), *E(spl)m β -LacZ* (E) and DHE (F).
- G Representative image of wing disks ($n > 10$ wing disks) bearing MARCM clones (marked by GFP) stained for Wg. In the *mRpl4^{K14608}* MARCM clones, *UAS-HA-wap* are expressed under the control of *tub-Gal4*.
- H Representative image of wings ($n > 15$ wings) from flies expressing *UAS-mnb-RNAi* under the control of *hh-Gal4*.
- I Representative image of wing disks ($n > 15$ wing disks) from flies expressing *UAS-mnb-RNAi* under the control of *hh-Gal4* that have been stained for Cut.

Data information: Representative clone is marked by white arrow in (G). Scale bars = 100 μ m.

Source data are available online for this figure.

To further investigate whether mRpl4 modulates Notch signaling in vertebrates, we analyzed the role of mRpl4 homolog in zebrafish, an excellent vertebrate model for developmental studies (Zhao et al, 2021). The zebrafish *mRpl4* (*zmRpl4*) null allele was generated using CRISPR-Cas9-mediated genome editing system. The isolated mutant allele, *zmRpl4^{mu}*, carries an indel (24-bp deletion and 2-bp insertion) that leads to frameshifting and premature translation termination. As a result, the mutant allele produces a small hybrid protein that retains the first 63 amino acids of wild-type *zmRpl4*, followed by 37 irrelevant amino acids (Fig EV5A). In the homozygous *zmRpl4^{mu}* mutant larvae, the mRNA level of *zmRpl4* was significantly decreased (Fig EV5B), indicating that the mutation inhibits transcript production and/or impairs the mRNA stability. Using quantitative real-time PCR analysis, we surveyed the expression level of several members of the Notch signaling pathway. In 5-

day postfertilization (dpf) larvae, the expression level of Notch signaling receptor gene, *notch1a*, and target genes, *hey1* and *her15.1*, was significantly reduced in the *zmRpl4^{mu}* mutant (Fig 7A). The expression of two other Notch target genes, *her4.1* and *her6*, was not affected (Fig EV5C). These observations suggest that Notch signaling lies genetically downstream of *zmRpl4* during zebrafish development. Next, we visualized the expression pattern of Notch signaling components by *in situ* hybridization. At 5 dpf, *zmRpl4* was highly expressed in the digestive system, mainly in the liver and intestinal bulb (Fig 7B). In consistent with previous studies (Lorent et al, 2004; Crosnier et al, 2005), *notch1a* (Fig 7C) and *hey1* (Fig 7D) were also expressed in the digestive system. When examined by whole-mount RNA hybridization, *notch1a* (Fig 7C) and *hey1* (Fig 7D) expression was found to be severely decreased in the *zmRpl4^{mu}* mutant larvae at 5 dpf. Taken together, these data

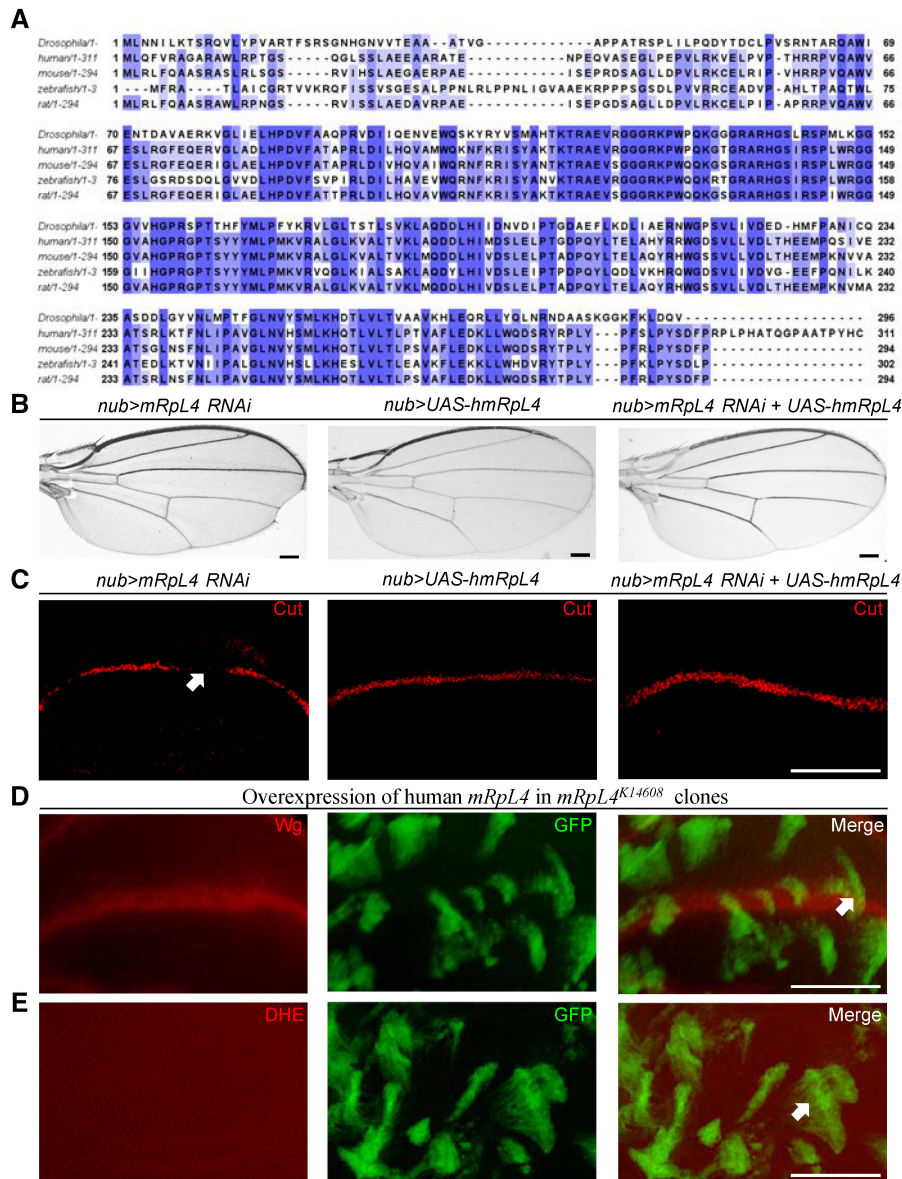


Figure 6. mRpl4 regulates Notch signaling in the *Drosophila* wing.

- A** Alignment of mRpl4 protein sequences from fly, human, mice, zebrafish and rat. The conserved residues are labeled with blue shadow.
- B** Representative images of wings ($n > 15$ wings) from flies expressing *mRpl4 RNAi*, *UAS-hmRpl4* and both under the control of *nub-Gal4*.
- C** Representative images of wing imaginal disks ($n > 10$ wing disks) stained for Cut from flies expressing *mRpl4 RNAi*, *UAS-hmRpl4* and both under the control of *nub-Gal4*. Representative regions showing Notch activity defects are marked by white arrow.
- D, E** Representative images of wing disks ($n > 10$ wing disks) bearing MARCM clones stained for Wg (D) and DHE (E). The MARCM clones are marked by GFP, and *UAS-hmRpl4* are expressed under the control of *tub-Gal4* in these clones.

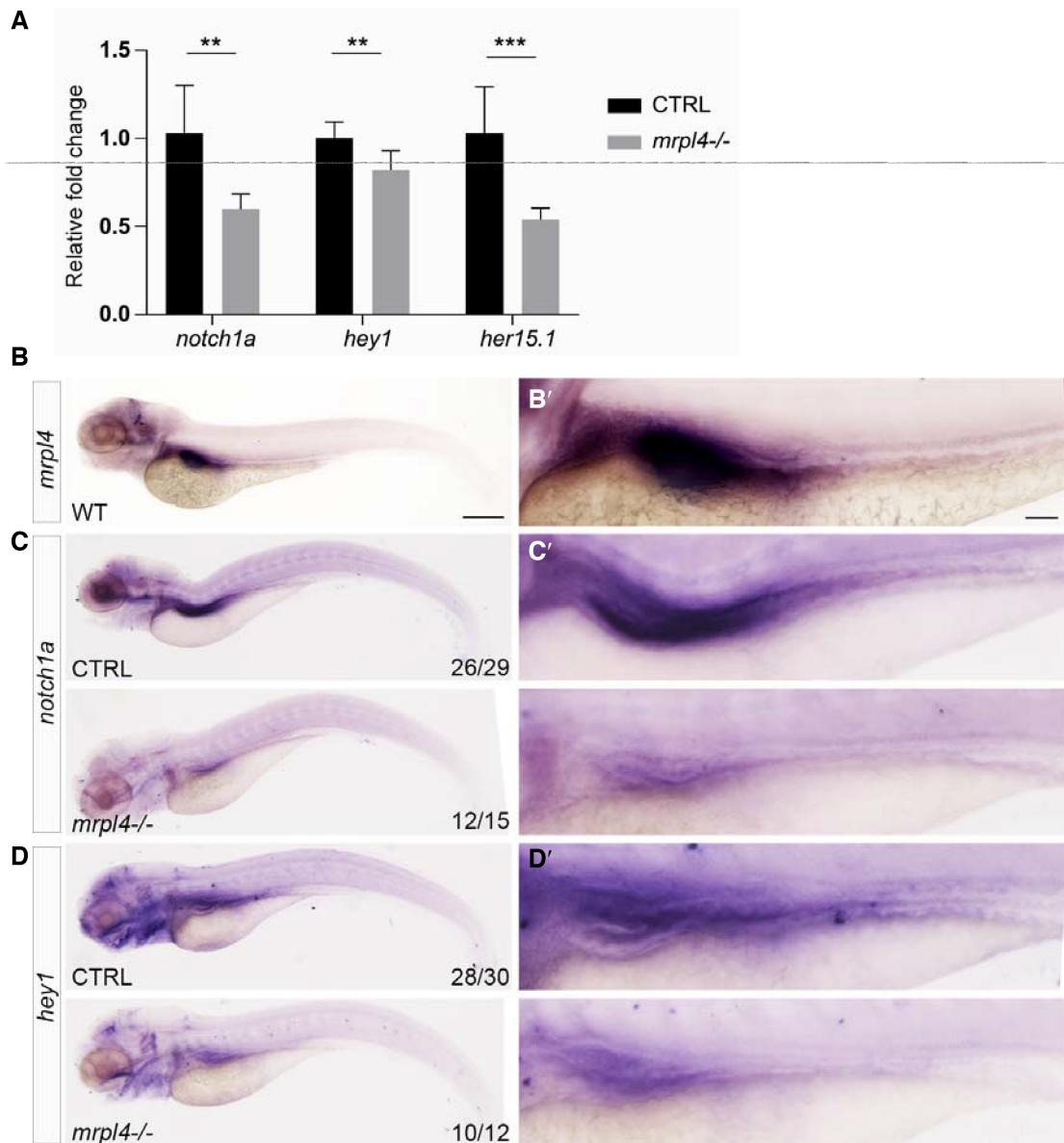
Data information: Representative clones are marked by white arrows (D, E). Scale bars = 100 μ m.

demonstrate that Notch signaling is also modulated by mRpl4 during zebrafish development.

Discussion

Mitochondrial ribosomal proteins are essential for animal development and have been implicated in developmental defects and

genetic disorders, but it is unknown whether and how MRPs could regulate Notch signaling. Here, we report that mRpl4 regulates Notch signaling activation downstream of NICD production during fly wing development. The observations that human mRpl4 protein rescues fly wing developmental defects and that zebrafish Notch signaling is also impacted in *zmRpl4* mutant indicate that this regulatory mode might be conserved in vertebrates. The WD40 repeat protein wap and the Ser/Thr protein kinase *mnb* provide a potential



link between mRpl4 and Su(H). Given that the only annotated domain of mRpl4 (ribosomal L4) functions to bind rRNA, it is difficult to interpret how mRpl4 exerts regulatory function on Su(H) protein. mRpl4 protein might possess undiscovered biochemical activity, but several clues suggest that the *mnb* kinase might be involved to modify Notch signaling. We found that, similar as mRpl4 and *wap*, *mnb* also positively regulates Notch signaling during fly wing development.

Both Su(H) and NICD bear conserved *mnb* phosphorylation consensus sequences, and the potential functional significance is discussed below. Phosphorylation at various sites impacts Su(H) protein stability and affinity with DNA, as well as the formation and dynamics of repressor or activator complex (Auer *et al.*, 2015; Nagel *et al.*, 2017; Frankenreiter *et al.*, 2021; Fechner *et al.*, 2022). The presumptive *mnb* target residue (T426) lies in the C-terminal domain (CTD) of Su(H), a region that is not involved in DNA binding

(Kovall & Hendrickson, 2004; Wilson & Kovall, 2006). Thus, although mRpl4 and wap might recruit mnb to phosphorylate Su(H), such modification will unlikely alter its affinity with chromosome. The T426 phosphorylation site resides in the conserved β -strand motif that interacts with the ankyrin repeats domain of NICD (Nam *et al.*, 2006; Choi *et al.*, 2012) and the transcription repressor Hairless (Yuan *et al.*, 2016). It is attempting to speculate that T426 phosphorylation could potentially affect the interaction of Su(H) with NICD and Hairless, which in turn may modulate the composition, stability, activity, and turnover of Su(H) transcription regulatory complexes. These hypotheses could help to explain the reduced occupation of Su(H) on Notch targets observed in mRpl4 RNAi wing disk cells. Interestingly, the mitogen-activated protein kinase (MAPK) phosphorylates Su(H) at P424 to attenuate Notch signaling (Auer *et al.*, 2015; Fechner *et al.*, 2022). The mnb and MAPK phosphorylation sites are in such close proximity, making it hard to ignore the potential antagonistic effect between them. At present, we could not rule out the possibility that mnb may also target less conserved consensus sites in other domains of Su(H) to modify its activity. Alternatively, unknown kinases that interact with wap could contribute to modification and regulation of Su(H). The vertebrate orthologs of mnb are known to phosphorylate NICD and attenuate Notch signaling (Fernandez-Martinez *et al.*, 2009; Hämmerle *et al.*, 2011; Morrugares *et al.*, 2020); whether mnb could phosphorylate NICD during fly development is still illusive. Further investigations are needed to reveal how mRpl4 and wap-mnb regulate Su(H) and Notch signaling activity.

Apart from the co-factors of transcription regulatory complexes, the heterogeneous nuclear ribonucleoprotein Hrb27/Hrp48 is a recently identified nuclear protein that regulates Notch signaling during fly wing development. Hrb27 utilizes at least two separate pathways to modulate Notch signaling. In female flies, Hrb27 represses the expression of the sex determination master gene *Sex-lethal* (*Sxl*) to ensure a proper amount of Notch during wing development (Suisa *et al.*, 2010). *Sxl* protein binds Notch mRNA and inhibits Notch protein translation in ovary cells (Penn & Schedl, 2007), but whether similar mode of action exists in wing disk cells has not been directly tested yet. In both males and females, Hrb27 interacts with the ubiquitin ligase Deltex (*Dx*) to attenuate Notch signaling activity in a *Sxl*-independent manner (Dutta *et al.*, 2017, 2020). Epistasis assays demonstrate that Hrb27 functions upstream of NICD in both pathways (Suisa *et al.*, 2010; Dutta *et al.*, 2017). In our hands, mRpl4 regulates Notch signaling activity in both sexes and likely functions downstream of NICD. We believe that Hrb27 and mRpl4 might not directly collaborate with each other to regulate Notch signaling.

Recent studies have begun to reveal that mitochondria and related proteins could regulate Notch signaling through various pathways. Mitochondrial fission factor Drp1 promotes Notch activation in fly ovariole follicle cells (Mitra *et al.*, 2012) and human breast cancer cells (Chen *et al.*, 2018b). Mitochondrial fusion proteins inhibit Notch activity in fly lymph gland (Ray *et al.*, 2021) and mouse embryonic heart (Cao *et al.*, 2016), but act to promote Notch activation in mouse neural stem cells (Khacho *et al.*, 2016). In fly neuroblasts, depletion of mitochondrial fusion protein Opa1, but not the other fusion protein Marf, leads to reduction of Notch pathway activity (Dubal *et al.*, 2022). These studies indicate that mitochondria morphology and Notch signaling might be generally associated

during animal development, but the mode of action varies significantly among different tissues. In several developmental events, the effects of mitochondria on Notch signaling are mediated by one of its major metabolites, ROS. Mitochondrial transcription factor A (TFAM) maintains cellular ROS production to activate Notch signaling during mouse keratinocytes differentiation (Hamanaka *et al.*, 2013). On the contrary, ROS inhibits Notch activity by triggering autophagic degradation of NICD in mouse hematopoietic stem cells (Cao *et al.*, 2016) and by inducing expression of inhibitory gene in mouse neural stem cells (Khacho *et al.*, 2016). In fly wing disk cells, burst of ROS stimulates TOR activity, which activates Notch signaling as a secondary response (Perez-Gomez *et al.*, 2020). Thus, ROS also impacts Notch signaling activity in a developmental context-dependent manner. Unlike in mouse keratinocytes, reduction of cellular ROS is insufficient to inhibit Notch activation in fly wing imaginal disk. We demonstrated that fly mRpl4 regulates Notch signaling through a separate route which is likely independent of OXPHOS protein synthesis, thus adding another layer to the complex regulatory network between mitochondria and Notch signaling.

Based on our findings and previous studies, we argue that the functional diversity of MRPs might be seriously underestimated. Increasing evidence indicates that MRPs perform common as well as separate functions during animal development. For the five MRPs we examined, all of them are required for ROS production in wing disk cells, but only mRpl4 regulates Notch signaling activity. During fly eye development, mRpl4 and mRpl17, but not mRps15 and mRpl12, are required for cell cycle progressing (Galloni, 2003; Frei *et al.*, 2005; Mandal *et al.*, 2005). Instead, mRpl12 possesses a unique ability to regulate cell growth in larval eye disk, wing disk, and fat body cells (Frei *et al.*, 2005). mRpl55 is essential for eye cell survival in the pupal stage, without affecting cell cycle nor cell growth in the larvae (Tselykh *et al.*, 2005). We noticed that mutation of *mRpl4* leads to the accumulation of cellular ROS in fly ovary follicle cells (Wang *et al.*, 2012), but results in reduction of ROS in wing disk (Fig 3A) and eye disk cells (Mandal *et al.*, 2005). Given that the same *mRpl4* allele is used, it is likely that mRpl4 regulates mitochondrial OXPHOS activity in a tissue-specific manner. The underlying mechanism and the biological significance of tissue-specific as well as component-specific functions of fly MRPs demand further investigation. We also looked into the ProteinAtlas database (www.proteinatlas.org; Thul *et al.*, 2017) to assess the expression pattern of vertebrate MRPs. The subcellular localization status of 58 human MRPs has been examined by immunofluorescence analysis, and about half of them (27/58) are found in cellular compartments other than mitochondria. Interestingly, around one third of these MRPs (19/58) are present within or nearby cell nucleus. As for mRpl4, no classical nuclear localization signal (NLS) motifs are found in fly and vertebrate proteins. However, a pat-7 type NLS (PDKRFRL) was identified in wap using the PSORT predication program (Horton *et al.*, 2007). It is possible that mRpl4 and other MRPs might be localized to distinct cellular compartments by their interacting partners. Therefore, in contrast to the general thoughts of being confined in the mitochondria to synthesis OXPHOS proteins, many MRPs may have “part-time jobs” in other cellular organelles. Comprehensive investigations of how MRPs regulate cell cycle, cell growth, and tissue development would help us to better understand their diverse functions.

Materials and Methods

Drosophila genetics

The Gal4-UAS system was utilized for tissue-specific gene expression. The *Hh*-Gal4, *Sgs*-Gal4 (Du et al, 2016), *nub*-Gal4 (Bloomington Drosophila Stock Center, BDSC 86108), and *1407*-Gal4 (BDSC 8751) stocks were used to drive transgene and RNAi expression. To induce mosaic clones, the following stocks were used: *Ubx-FLP;Ubi-mRFP, FRT40A*; *Ubx-FLP;Ubi-GFP, FRT40A* and *Ubx-FLP; FRT82B, Ubi-mRFP*. The MARCM experiments were performed with the *hs-FLP, tub-GAL4, UAS-GFP; tub-GAL80, FRT40A* stock. We used *mRpl4^{K14608}, FRT40A* (Kyoto Stock Center, KSC 111435), *FRT82B, CoVa^{tend}* (BDSC 33839), *FRT42D, mRps28^{k13104}* (KSC 111025) and *mRpl24¹⁰⁶⁶⁹², FRT40A* (KSC 114548) for genetic analysis. The *NRE-GFP* (BDSC 30728) and *E(spl)mβ-LacZ* (Yu et al, 2013) reporters were used to visualize Notch signaling activity. The RNAi lines used in this work are as follows: *UAS-mRpl4 RNAi* (Vienna Drosophila Resource Center, VDRC 101351), *UAS-wap RNAi* (VDRC 107076), *UAS-mnb RNAi* (VDRC 107066), *UAS-CoVa RNAi* (VDRC 109070), *UAS-CoVa RNAi-2* (BDSC 58282), *UAS-mRps2 RNAi* (National Institute of Genetics, Japan, 2937R-1), *UAS-mRps12 RNAi* (BDSC 38251), *UAS-ND-42 RNAi* (BDSC 58282), *UAS-mRpl24 RNAi* (VDRC 103782), *UAS-mRps28 RNAi* (VDRC 107181), *UAS-ND-15.6 RNAi* (Tsinghua Fly Center, THFC 1766), *UAS-Pdsw RNAi* (THFC 3175), and *UAS-ND-19 RNAi* (THFC 4895). The transgenic lines used in this work are as follows: *UAS-Delta* (BDSC 26695), *UAS-Serrate* (BDSC 5815), *UAS-N^{FL}* (BDSC 26820), *UAS-NEXT* (BDSC 63220), and *UAS-NICD* (Go et al, 1998). The *Su(H)*-GFP and *mnb*-GFP stocks carried BAC transgenes that express GFP-tagged fusion proteins under the control of their genomic regulatory sequence (Sarov et al, 2016). The *Su(H)*-lacZ; *Esg*-Gal4, *UAS-mCD8-GFP, tub-Gal80^{TS}* stock was used to monitor Notch signal activity in adult midgut cells (Zhao et al, 2022).

The somatic mosaic screening was performed by crossing the Bruinfly mutant stocks (Chen et al, 2005) with virgin females bearing *Ubx-Flp* and corresponding FRT site. The wing morphology of the progenies was examined, and mutants that resulted in wing margin nicks were selected for secondary screen. The Notch signaling activity was monitored in third instar larval wing imaginal disks in the secondary screen (Ren et al, 2018). For MARCM analysis, virgin females of *mRpl4^{K14608}, FRT40A* were first crossed with desirable transgenic strain and males of the progeny were picked to mate with the *FRT40A* MARCM stock. Three-day-old larval from the second cross were then heat-shocked at 37°C for 1 h using water bath to induce clones.

Generation of transgenic flies

Total RNAs were extracted from third instar larvae with TRIeasy reagent (Yeasen Biotech, Shang Hai, China) and followed by cDNA synthesis with Hifair First Strand cDNA Synthesis Kit (Yeasen Biotech). Sequence-specific primers (Appendix Table S1) were designed to amplify cDNA fragments of fly *mRpl4* and *wap* by High-Fidelity Master Mix (Molecular Cloning Laboratories, MCLAB). Human *mRpl4* ortholog was amplified from a cDNA clone provided by Dr. Jiahuai Han. The cDNAs were subcloned into pUAST-attB vector using EcoR I and Kpn I sites by ClonExpress II One Step Cloning Kit

(Vazyme). The transgenic flies were generated by phiC31 integrase-mediated site-specific insertion at the left arm of third chromosome with cytogenetic location at 68A4. The embryonic injections were performed by Core Facility of Drosophila Resource and Technology at the Center for Excellence in Molecular Cell Science, Chinese Academy of Sciences (Shanghai, China) and Fungene Biotechnology (Qidong, Jiangshu Province, China).

Immunofluorescence staining

Third instar larvae were dissected in ice-cold PBS and fixed in 4% paraformaldehyde for 15 min and then washed in PBST (PBS containing 0.1% Triton X-100) for 15 min. The larvae were blocked in PBST with 0.2% BSA for 1 h before incubating with primary antibodies overnight at 4°C. The following primary antibodies were used: mouse anti-Cut (1:200; 2B10; Developmental Studies Hybridoma Bank, DSHB), mouse anti-Wingless (1:200; 4D4; DSHB), mouse anti-Notch intracellular domain (1:200; C17.9C6; DSHB), mouse anti-Delta (1:200; C594.9B; DSHB), rabbit anti-LacZ (1:4000; Cappel), and rabbit anti-GFP (1:50; G10362; Thermo Fisher). Alexa flour-conjugated secondary antibodies (1:400; Invitrogen) were used. Wing disks and adult midguts were dissected and mounted in 40% glycerol for imaging.

Dihydroethidium staining

We monitored cellular ROS level in wing disks by DHE staining (Robinson et al, 2006). Third instar larvae were incubated for 10 min at 22°C in SFX-Insect medium (HyClone) containing 8 μM DHE (Sigma) and then rinsed twice in SFX-Insect medium before fixed in 4% paraformaldehyde for 5 min. The wing disks were rinsed once with PBS and mounted in 40% glycerol.

Generation of mRpl4 antibody

A rabbit polyclonal antibody was generated against a synthetic peptide (DYTDCLPVSRRNTARQAW) corresponding to amino acids 52–68 of the *Drosophila* mRpl4 protein (ABclonal, Wuhan, China). The specificity of rabbit antisera was examined by immunoblotting (1:2,000) using protein lysates extracted from wild-type and *mRpl4* RNAi-expressing wing disks (Fig 5A). Note that this antibody is not suitable for immunofluorescence.

Biochemistry

Third instar larval brain and imaginal disks were lysed in RIPA buffer (150 mM sodium chloride [NaCl], 1.0% NP-40, 0.5% sodium deoxycholate, 0.1% sodium dodecyl sulfate [SDS], 50 mM Tris-HCl, pH 8.0) supplemented with protease inhibitor cocktail (20124ES10; Yeasen Biotech). Immunoblotting analyses were carried out using standard protocols. The following antibodies were used for immunoblotting: mouse anti-α-Tubulin (1:5,000; A11126; Thermo Fisher), mouse anti-β-Tubulin (1:1,000; E7; DSHB), rabbit anti-GAPDH (1:2,000; sc25778; Santa Cruz), rabbit anti-HA (1:5,000; 3,724; Cell Signaling), mouse anti-FLAG (1:5,000; F1804; Thermo Fisher), rabbit anti-GFP (1:400; G10362; Thermo Fisher), rabbit anti-mRpl4 (1:2,000; E6023; ABclonal), and mouse anti-Histone3 (1:20,000; BE3015; EasyBio, Beijing, China).

Immunoprecipitations were performed using anti-HA agarose (E6779; Sigma) and magnetic anti-GFP beads (GNM-25-1000; Lablead) according to the manufacturer's instructions. Third instar larval brain and imaginal disks were lysed in NP-40 buffer (150 mM sodium chloride [NaCl], 1.0% NP-40, 50 mM Tris-HCl, pH 8.0) supplemented with protease inhibitor cocktail (20124ES10; Yeasen Biotech).

Subcellular fractionations were separated as previously described with minor modification (Du *et al*, 2016). Briefly, larval brain and imaginal wing disks were collected at 1,250 g for 10 min and washed in PBS before lysed in Buffer I (15 mM Hepes pH 7.4, 10 mM KCl, 5 mM MgCl₂, 0.2 mM EDTA, 1 mM DTT) for 30 min on ice to generate the cytoplasmic fraction. Nuclei were pelleted at 3,000 g for 10 min and washed twice in Buffer I before resuspended in Buffer II (50 mM Hepes, pH 7.6, 110 mM KCl, 150 mM NaCl, 1% Triton X-100, 10% glycerol, 1 mM DTT, 0.1 mM EDTA) for nuclear protein extraction. The precipitate is removed by centrifugation at 5,000 g for 10 min. All lysis buffers were supplemented with protease inhibitor cocktail (20124ES10; Yeasen Biotech).

Mounting of adult fly wings

Adult flies with correct genotypes were collected and fixed overnight in isopropanol. Dissected adult wings were mounted in Euparal mounting media (BioQuip).

Yeast two-hybridization

Yeast two-hybridization was performed with the Matchmaker Gold Yeast Two-Hybrid System (Takara, 630489). The *mRpl4* cDNAs were cloned into pGBKT7 vector using Nde I and EcoR I sites by ClonExpress II One Step Cloning Kit (Vazyme) and expressed as a fusion to the Gal4 DNA-binding domain as bait protein. We confirmed that the mRpl4 bait does not autonomously activate the reporter genes in the absence of a prey protein. A concentrated overnight culture of the bait strain was combined with the Mate & Plate Library—Universal Drosophila (Takara, 630485) strain and incubated at 30°C for 20–24 h with slowly shaking (30 rpm) to allow mating between the two strains. Presence of yeast zygotes was examined under a phase contrast microscope (40×), and the mated culture was spread on agar plates with double dropout media containing 40 µg/ml X-alpha-Gal and 200 ng/ml Aureobasidin A (DDO/X/A). All the blue colonies that grew on DDO/X/A were transferred to higher stringency agar plates with quadruple dropout media containing 40 µg/ml X-alpha-Gal and 200 ng/ml Aureobasidin A (QDO/X/A). The QDO/X/A positive clones were further analyzed to verify the interactions and identify the insert in the prey plasmid. Two candidate preys were isolated, and the cDNA inserts were sequenced.

Chromatin immunoprecipitation (ChIP)

The ChIP experiments from wing imaginal disks were performed based on previously described protocols (Krejci & Bray, 2007; Du *et al*, 2016). Roughly, 2000 wing disks were dissected in ice-cold SFX-insect medium for each genotype. After fixation in 1.8% formaldehyde on a rotating wheel at room temperature for 15 min, disks were divided into two parts for fragmentation by sonication

(ON = 30 s, OFF = 1 min, high power, 4 times). The size of bulk DNA fragments ranges from 100 to 300 bp. Mouse monoclonal antibody against Su(H) (sc398453, Santa Cruz Biotechnology) was used for immunoprecipitation. The Perfect Start Green qPCR Super Mix (TransGen Biotech) was used for real-time quantitative PCR experiments conducted on an ABI QuantStudio 6 Flex System (Thermo Fisher, USA). Primers are designed to cover the Su(H) binding sites in the regulatory regions of *cut*, *Wg*, *vestigial*, and *E(Spl)* family genes (Bailey & Posakony, 1995; Lecourtois & Schweisguth, 1995; Klein & Arias, 1999; Krejci & Bray, 2007). The sequences of primers are shown in Appendix Table S1. The value of % Input was calculated by the following formula: % Input = $100 \times 2^{-(C_t[\text{ChIP}] - C_t[\text{Input}] - \text{Log}_2(\text{Input Dilution Factor}))}$.

Generation of zebrafish *zmRpl4* mutant allele

The zebrafish *zmRpl4* mutant line was generated using the CRISPR/Cas9 system. Potential CRISPR target sites were screened on the CRISPRscan website (<https://www.crisprscan.org/>). To generate the F0 generation of mutants, 200 pg *zmRpl4* guide RNA (targeting sequence 5'-GGGCTGGTGTCAAGTGAGCT-3', located in the 3rd exon) and 200 pg Cas9 mRNA were co-injected into wild-type embryos at one-cell stage. The F1 generation was genotyped by PCR amplifying a genomic DNA fragment harbored the *zmRpl4* target site and subsequent sequencing. The *zmRpl4* mutant allele was identified, containing a 24-base pair (bp) deletion and a 2-bp insertion at exon 3 (Fig EV5A).

qRT-PCR

Wing imaginal disks were dissected from third instar larvae, and total RNAs were extracted by TRIeasy reagent (Yeasen Biotech), followed by cDNA synthesis with Hifair First Strand cDNA Synthesis Kit (Yeasen Biotech). Around 200 wing disks were collected for each genotype. The Perfect Start Green qPCR Super Mix (TransGen) was used for real-time quantitative PCR experiments conducted on an ABI QuantStudio 6 Flex System (Thermo Fisher). For zebrafish experiments, 5 dpf wild-type and *zmRpl4* mutant larvae were collected for each biological replicate, and total RNA was isolated using the TRNzol Universal (TIANGEN, China), following reverse transcription into cDNA using TransScript[®] Uni All-in-One First-Strand cDNA Synthesis SuperMix system (TransGen) according to the manufacturer's protocol. The quantitative PCR was performed using PerfectStart[®] Green qPCR SuperMix (TransGen) with a QuantStudio[™] 3 Real-Time PCR Instrument (Applied Biosystems). The expression of β-actin was used for normalization to calculate fold differences in selected transcripts between experimental groups. The sequence of qPCR primers used in this study is provided in Appendix Table S1.

Zebrafish whole-mount *in situ* hybridization

At 5 dpf, zebrafish larvae were fixed in 4% paraformaldehyde (PFA) at 4°C overnight and rinsed in PBST (0.1% Tween-20 in PBS) following subsequently dehydrated in methanol and stored at -20°C. The whole-mount *in situ* hybridization was performed as described previously (Thisse & Thisse, 2008). To generate antisense riboprobes of *mrpl4* and *hey1*, cDNA fragments were amplified (the

sequence of primers was provided in Appendix Table S1) and cloned into pEASY-T3 (TransGen Biotech) and TOPO (Life Technologies) vectors, respectively. The plasmids containing *zmRpL4*, *hey1*, and *notch1a* (Zhao et al, 2014) cDNA fragments were linearized, and the digoxigenin-labeled antisense RNA riboprobes were *in vitro* transcribed using a DIG RNA Labeling Kit (Roche). The hybridized probes were detected with alkaline-phosphatase-conjugated anti-digoxigenin antibody (Roche), and the signal was developed with BM purple (Roche).

Image capture and processing

The fluorescence images were acquired with a Leica SP8 confocal microscope and processed in Photoshop and ImageJ. The following detection wavelengths were used: 510–530 nm for Alexa 488, 525–550 nm for GFP, 580–600 nm for RFP, and 590–610 nm for Alexa 568. The images of adult wings were acquired with a Leica DMIL inverted microscope equipped with a QImaging QICAM Fast 1394 digital camera. Minor image adjustments (overall brightness and/or contrast) were performed in Photoshop and Microsoft PowerPoint.

Statistics

All genetic experiments were performed independently at least two times, and independent but genetically identical samples were used. For adult wing phenotypes, at least 30 flies were analyzed. For wing imaginal disk staining, at least 10 disks were examined for each genotype. For qRT-PCR analysis, three biological repeats were performed. Error bars show mean \pm standard error of measurement. Boxplots show median (thick line in the box) and maximum values (whiskers). Statistical significance was tested using two-tailed unpaired *t*-test. *P*-value was indicated as follows: **P* < 0.05, N.S., not significant.

Data availability

This study includes no data deposited in external repositories.

Expanded View for this article is available [online](#).

Acknowledgments

We would like to thank Drs. Alan Jian Zhu, Renjie Jiao, Zhouhua Li, Wei Wu, the Bloomington Stock Center, the Kyoto Fly Stock Center, the Tsinghua Fly Stock Center, the Vienna Drosophila Resource Center, National Institute of Genetics (NIG), and the Developmental Studies Hybridoma Bank (DSHB) for fly stocks and antibodies. We thank Dr. Jiahui Han for providing human mRpL4 cDNA clone. We thank Haomiao Li for helping with adult fly gut experiments. We thank Core Facility of Drosophila Resource and Technology, CEMCS, CAS, and Fungene Biotechnology (Qidong, Jiangsu Province, China) for generation of transgenic fly strains. This work was supported by the National Natural Science Foundation of China (31970478 and 31772526 to J.Z.; 32030012 and 31872295 to J.S.; 31970506 and 32170541 to L.Z.).

Author contributions

Dongqing Mo: Data curation; formal analysis; investigation; writing – original draft. **Chenglin Liu:** Data curation; formal analysis; investigation. **Yao Chen:** Data curation; formal analysis; validation. **Xinkai Cheng:** Data curation; formal analysis; investigation. **Jie Shen:** Conceptualization; supervision;

funding acquisition; project administration; writing – review and editing. **Long Zhao:** Conceptualization; funding acquisition; project administration; writing – review and editing. **Junzheng Zhang:** Conceptualization; supervision; project administration; writing – review and editing.

Disclosure and competing interests statement

The authors declare that they have no conflict of interest.

References

- Amikura R, Kashikawa M, Nakamura A, Kobayashi S (2001) Presence of mitochondria-type ribosomes outside mitochondria in germ plasm of *Drosophila* embryos. *Proc Natl Acad Sci USA* 98: 9133–9138
- Auer JS, Nagel AC, Schulz A, Wahl V, Preiss A (2015) MAPK-dependent phosphorylation modulates the activity of suppressor of hairless in *Drosophila*. *Cell Signal* 27: 115–124
- Bailey AM, Posakony JW (1995) Suppressor of hairless directly activates transcription of *Enhancer of split* complex genes in response to Notch receptor activity. *Genes Dev* 9: 2609–2622
- Basak NP, Roy A, Banerjee S (2014) Alteration of mitochondrial proteome due to activation of Notch1 signaling pathway. *J Biol Chem* 289: 7320–7334
- Bray SJ (2006) Notch signalling: a simple pathway becomes complex. *Nat Rev Mol Cell Bio* 7: 678–689
- Cao Y, Fang Y, Cai J, Li X, Xu F, Yuan N, Zhang S, Wang J (2016) ROS functions as an upstream trigger for autophagy to drive hematopoietic stem cell differentiation. *Hematology* 21: 613–618
- Chen J, Call GB, Beyer E, Bui C, Cespedes A, Chan A, Chan J, Chan S, Chhabra A, Dang P et al (2005) Discovery-based science education: functional genomic dissection in *Drosophila* by undergraduate researchers. *PLoS Biol* 3: e59
- Chen A, Tiosano D, Guran T, Baris HN, Bayram Y, Mory A, Shapiro-Kulnane L, Hodges CA, Akdemir ZC, Turan S et al (2018a) Mutations in the mitochondrial ribosomal protein MRPS22 lead to primary ovarian insufficiency. *Hum Mol Genet* 27: 1913–1926
- Chen L, Zhang J, Lyu Z, Chen Y, Ji X, Cao H, Jin M, Zhu J, Yang J, Ling R et al (2018b) Positive feedback loop between mitochondrial fission and notch signaling promotes survivin-mediated survival of TNBC cells. *Cell Death Dis* 9: 1050
- Cheong A, Archambault D, Degani R, Iverson E, Tremblay KD, Mager J (2020) Nuclear-encoded mitochondrial ribosomal proteins are required to initiate gastrulation. *Development* 147: dev188714
- Choi SH, Wales TE, Nam Y, O'Donovan DJ, Sliz P, Engen JR, Blacklow SC (2012) Conformational locking upon cooperative assembly of Notch transcription complexes. *Structure* 20: 340–349
- Crosnier C, Vargesson N, Gschmeissner S, Ariza-McNaughton L, Morrison A, Lewis J (2005) Delta-notch signalling controls commitment to a secretory fate in the zebrafish intestine. *Development* 132: 1093–1104
- Dai SH, Wu QC, Zhu RR, Wan XM, Zhou XL (2020) Notch1 protects against myocardial ischaemia-reperfusion injury via regulating mitochondrial fusion and function. *J Cell Mol Med* 24: 3183–3191
- Degoutin JL, Milton CC, Yu E, Tipping M, Bosveld F, Yang L, Bellaiche Y, Veraksa A, Harvey KF (2013) Riquiqui and minibrain are regulators of the hippo pathway downstream of Dachsous. *Nat Cell Biol* 15: 1176–1185
- Du J, Zhang J, He T, Li Y, Su Y, Tie F, Liu M, Harte PJ, Zhu AJ (2016) Stuxnet facilitates the degradation of Polycomb protein during development. *Dev Cell* 37: 507–519
- Dubal D, Moghe P, Verma RK, Uttakar B, Rikhy R (2022) Mitochondrial fusion regulates proliferation and differentiation in the type II neuroblast lineage in *Drosophila*. *PLoS Genet* 18: e1010055

- Dutta D, Paul MS, Singh A, Mutsuddi M, Mukherjee A (2017) Regulation of notch signaling by the heterogeneous nuclear ribonucleoprotein Hrp48 and Deltex in *Drosophila melanogaster*. *Genetics* 206: 905–918
- Dutta D, Mutsuddi M, Mukherjee A (2020) Regulation of notch signaling in *Drosophila melanogaster*: the role of the heterogeneous nuclear ribonucleoprotein Hrp48 and Deltex. *Adv Exp Med Biol* 1227: 95–105
- Fechner J, Ketelhut M, Maier D, Preiss A, Nagel AC (2022) The binding of CSL proteins to either co-activators or co-repressors protects from proteasomal degradation induced by MAPK-dependent phosphorylation. *Int J Mol Sci* 23: 12336
- Fernandez-Martinez J, Vela EM, Tora-Ponsioen M, Ocaña OH, Nieto MA, Galceran J (2009) Attenuation of notch signalling by the Down-syndrome-associated kinase DYRK1A. *J Cell Sci* 122: 1574–1583
- Ferrari A, Del'Olivo S, Barrientos A (2021) The diseased mitoribosome. *FEBS Lett* 595: 1025–1061
- Frankenreiter L, Gahr BM, Schmid H, Zimmermann M, Deichsel S, Hoffmeister P, Turkiewicz A, Borggreve T, Oswald F, Nagel AC (2021) Phospho-site mutations in transcription factor suppressor of hairless impact notch signaling activity during hematopoiesis in *Drosophila*. *Front Cell Dev Biol* 9: 658820
- Frei C, Galloni M, Hafen E, Edgar BA (2005) The *Drosophila* mitochondrial ribosomal protein mRpl12 is required for cyclin D/Cdk4-driven growth. *EMBO J* 24: 623–634
- Galloni M (2003) Bonsai, a ribosomal protein S15 homolog, involved in gut mitochondrial activity and systemic growth. *Dev Biol* 264: 482–494
- Go MJ, Eastman DS, Artavanis-Tsakonas S (1998) Cell proliferation control by notch signaling in *Drosophila* development. *Development* 125: 2031–2040
- Gomez-Lamarca MJ, Falo-Sanjuan J, Stojnic R, Abdul Rehman S, Muresan L, Jones ML, Pillidge Z, Cerda-Moya G, Yuan Z, Baloul S et al (2018) Activation of the notch signaling pathway *in vivo* elicits changes in CSL nuclear dynamics. *Dev Cell* 44: 611–623
- Guruharsha KG, Kankel MW, Artavanis-Tsakonas S (2012) The Notch signalling system: recent insights into the complexity of a conserved pathway. *Nat Rev Genet* 13: 654–666
- Hamanaka RB, Glasauer A, Hoover P, Yang S, Blatt H, Mullen AR, Getsios S, Gottardi CJ, DeBerardinis RJ, Lavker RM et al (2013) Mitochondrial reactive oxygen species promote epidermal differentiation and hair follicle development. *Sci Signal* 6: ra8
- Hämmerle B, Ulin E, Guimera J, Becker W, Guillemot F, Tejedor FJ (2011) Transient expression of Mnb/Dyrk1a couples cell cycle exit and differentiation of neuronal precursors by inducing p27KIP1 expression and suppressing Notch signaling. *Development* 138: 2543–2554
- Han J, An O, Hong H, Chan THM, Song Y, Shen H, Tang SJ, Lin JS, Ng VHE, Tay DJT et al (2020) Suppression of adenosine-to-inosine (A-to-I) RNA editome by death associated protein 3 (DAP3) promotes cancer progression. *Sci Adv* 6: eaba5136
- Henrique D, Schweisguth F (2019) Mechanisms of notch signaling: a simple logic deployed in time and space. *Development* 146: dev172148
- Horton P, Park KJ, Obayashi T, Fujita N, Harada H, Adams-Collier CJ, Nakai K (2007) WoLF PSORT: protein localization predictor. *Nucleic Acids Res* 35: W585–W587
- Huang G, Li H, Zhang H (2020) Abnormal expression of mitochondrial ribosomal proteins and their encoding genes with cell apoptosis and diseases. *Int J Mol Sci* 21: 8879
- Kasahara A, Cipolat S, Chen Y, Dorn GW 2nd, Scorrano L (2013) Mitochondrial fusion directs cardiomyocyte differentiation via calcineurin and Notch signaling. *Science* 342: 734–737
- Khacho M, Clark A, Svoboda DS, Azzi J, MacLaurin JG, Meghaizel C, Sesaki H, Lagace DC, Germain M, Harper ME et al (2016) Mitochondrial dynamics impacts stem cell identity and fate decisions by regulating a nuclear transcriptional program. *Cell Stem Cell* 19: 232–247
- Klein T, Arias AM (1999) The vestigial gene product provides a molecular context for the interpretation of signals during the development of the wing in *Drosophila*. *Development* 126: 913–925
- Kovall RA, Hendrickson WA (2004) Crystal structure of the nuclear effector of notch signaling, CSL, bound to DNA. *EMBO J* 23: 3441–3451
- Krejčí A, Bray S (2007) Notch activation stimulates transient and selective binding of Su(H)/CSL to target enhancers. *Genes Dev* 21: 1322–1327
- Kummer E, Ban N (2021) Mechanisms and regulation of protein synthesis in mitochondria. *Nat Rev Mol Cell Biol* 22: 307–325
- Kung-Chun Chiu D, Pui-Wah Tse A, Law CT, Ming-Jing Xi, Lee D, Chen M, Kit-Ho Lai R, Wai-Hin Yuen V, Wing-Sum Cheu J, Wai-Hung Ho D et al (2019) Hypoxia regulates the mitochondrial activity of hepatocellular carcinoma cells through HIF/HEY1/PINK1 pathway. *Cell Death Dis* 10: 934
- Landor SK, Mutvei AP, Mamaeva V, Jin S, Busk M, Borra R, Grönroos TJ, Kronqvist P, Lendahl U, Sahlgren CM (2011) Hypo- and hyperactivated notch signaling induce a glycolytic switch through distinct mechanisms. *Proc Natl Acad Sci USA* 108: 18814–18819
- Lecourtis M, Schweisguth F (1995) The neurogenic suppressor of hairless DNA-binding protein mediates the transcriptional activation of the *Enhancer of split* complex genes triggered by notch signaling. *Genes Dev* 9: 2598–2608
- Lee SY, Long F (2018) Notch signaling suppresses glucose metabolism in mesenchymal progenitors to restrict osteoblast differentiation. *J Clin Invest* 128: 5573–5586
- Lee T, Luo L (2001) Mosaic analysis with a repressible cell marker (MARCM) for *Drosophila* neural development. *Trends Neurosci* 24: 251–254
- Lee KS, Wu Z, Song Y, Mitra SS, Feroze AH, Cheshier SH, Lu B (2013) Roles of PINK1, mTORC2, and mitochondria in preserving brain tumor-forming stem cells in a noncanonical notch signaling pathway. *Genes Dev* 27: 2642–2647
- Liao TS, Call GB, Guptan P, Cespedes A, Marshall J, Yackle K, Owusu-Ansah E, Mandal S, Fang QA, Goodstein GL et al (2006) An efficient genetic screen in *Drosophila* to identify nuclear-encoded genes with mitochondrial function. *Genetics* 174: 525–533
- Liu K, Shen D, Shen J, Gao SM, Li B, Wong C, Feng W, Song Y (2017) The super elongation complex drives neural stem cell fate commitment. *Dev Cell* 40: 537–551
- Lorent K, Yeo SY, Oda T, Chandrasekharappa S, Chitnis A, Matthews RP, Pack M (2004) Inhibition of jagged-mediated notch signaling disrupts zebrafish biliary development and generates multi-organ defects compatible with an Alagille syndrome phenocopy. *Development* 131: 5753–5766
- Ludikhuize MC, Meerlo M, Gallego MP, Xanthakis D, Burgaya Julià M, Nguyen NTB, Brombacher EC, Liv N, Maurice MM, Paik JH et al (2020) Mitochondria define intestinal stem cell differentiation downstream of a FOXO/notch axis. *Cell Metab* 32: 889–900
- Mandal S, Guptan P, Owusu-Ansah E, Banerjee U (2005) Mitochondrial regulation of cell cycle progression during development as revealed by the tenured mutation in *Drosophila*. *Dev Cell* 9: 843–854
- Marygold SJ, Roote J, Reuter G, Lambertsson A, Ashburner M, Millburn GH, Harrison PM, Yu Z, Kenmochi N, Kaufman TC et al (2007) The ribosomal protein genes and *minute* loci of *Drosophila melanogaster*. *Genome Biol* 8: R216
- Mitra K, Rikhy R, Lilly M, Lippincott-Schwartz J (2012) DRP1-dependent mitochondrial fission initiates follicle cell differentiation during *Drosophila* oogenesis. *J Cell Biol* 197: 487–497

- Mo D, Shen J, Zhang J (2022) Use of FLP/FRT system to screen for notch signaling regulators in the *Drosophila* wing. *Methods Mol Biol* 2472: 39–48
- Morrugares R, Correa-Sáez A, Moreno R, Garrido-Rodríguez M, Muñoz E, de la Vega L, Calzado MA (2020) Phosphorylation-dependent regulation of the Notch1 intracellular domain by dual-specificity tyrosine-regulated kinase 2. *Cell Mol Life Sci* 77: 2621–2639
- Nagel AC, Auer JS, Schulz A, Pfannstiel J, Yuan Z, Collins CE, Kovall RA, Preiss A (2017) Phosphorylation of suppressor of hairless impedes its DNA-binding activity. *Sci Rep* 7: 11820
- Nam Y, Sliz P, Song L, Aster JC, Blacklow SC (2006) Structural basis for cooperativity in recruitment of MAML coactivators to notch transcription complexes. *Cell* 124: 973–983
- Ohsawa S, Sato Y, Enomoto M, Nakamura M, Betsumiyama A, Igaki T (2012) Mitochondrial defect drives non-autonomous tumour progression through hippo signalling in *Drosophila*. *Nature* 490: 541–551
- Ojha R, Tantray I, Rimal S, Mitra S, Cheshier S, Lu B (2022) Regulation of reverse electron transfer at mitochondrial complex I by unconventional notch action in cancer stem cells. *Dev Cell* 57: 260–276
- Owusu-Ansah E, Yavari A, Mandal S, Banerjee U (2008) Distinct mitochondrial retrograde signals control the G1-S cell cycle checkpoint. *Nat Genet* 40: 356–361
- Penn JK, Schedl P (2007) The master switch gene sex-lethal promotes female development by negatively regulating the N-signaling pathway. *Dev Cell* 12: 275–286
- Perez-Gomez R, Magnin V, Mihajlovic Z, Slaninova V, Krejčí A (2020) Downregulation of respiratory complex I mediates major signalling changes triggered by TOR activation. *Sci Rep* 10: 4401
- Perumalsamy LR, Nagala M, Sarin A (2010) Notch-activated signaling cascade interacts with mitochondrial remodeling proteins to regulate cell survival. *Proc Natl Acad Sci USA* 107: 6882–6887
- Quiros PM, Mottis A, Auwerx J (2016) Mitonuclear communication in homeostasis and stress. *Nat Rev Mol Cell Biol* 17: 213–226
- Ray A, Kamat K, Inamdar MS (2021) A conserved role for Asrij/OCIAD1 in progenitor differentiation and lineage specification through functional interaction with the regulators of mitochondrial dynamics. *Front Cell Dev Biol* 9: 643444
- Ren L, Mo D, Li Y, Liu T, Yin H, Jiang N, Zhang J (2018) A genetic mosaic screen identifies genes modulating notch signaling in *Drosophila*. *PLoS One* 13: e0203781
- Richter-Dennerlein R, Dennerlein S, Rehling P (2015) Integrating mitochondrial translation into the cellular context. *Nat Rev Mol Cell Biol* 16: 586–592
- Robinson KM, Janes MS, Pehar M, Monette JS, Ross MF, Hagen TM, Murphy MP, Beckman JS (2006) Selective fluorescent imaging of superoxide *in vivo* using ethidium-based probes. *Proc Natl Acad Sci USA* 103: 15038–15043
- Saj A, Arziman Z, Stempfle D, van Belle W, Sauder U, Horn T, Dürrenberger M, Paro R, Boutros M, Merdes G (2010) A combined *ex vivo* and *in vivo* RNAi screen for notch regulators in *Drosophila* reveals an extensive notch interaction network. *Dev Cell* 18: 862–876
- Sarov M, Barz C, Jambor H, Hein MY, Schmied C, Suchold D, Stender B, Janosch S, K J VV, Krishnan RT et al (2016) A genome-wide resource for the analysis of protein localisation in *Drosophila*. *Elife* 5: e12068
- Suissa Y, Kalifa Y, Dinur T, Graham P, Deshpande G, Schedl P, Gerlitz O (2010) Hrp48 attenuates Sxl expression to allow for proper notch expression and signaling in wing development. *Proc Natl Acad Sci USA* 107: 6930–6935
- Thisse C, Thisse B (2008) High-resolution *in situ* hybridization to whole-mount zebrafish embryos. *Nat Protoc* 3: 59–69
- Thörig GE, Heinstra PW, Scharloo W (1981a) The action of the notch locus in *Drosophila melanogaster*. II. Biochemical effects of recessive lethals on mitochondrial enzymes. *Genetics* 99: 65–74
- Thörig GE, Heinstra PW, Scharloo W (1981b) The action of the notch locus in *Drosophila melanogaster*. I. Effects of the notch8 deficiency on mitochondrial enzymes. *Mol Gen Genet* 182: 31–38
- Thul PJ, Åkesson L, Wiking M, Mahdessian D, Geladaki A, Ait Blal H, Alm T, Asplund A, Björk L, Breckels LM et al (2017) A subcellular map of the human proteome. *Science* 356: eaal3321
- Tselykh TV, Roos C, Heino TI (2005) The mitochondrial ribosome-specific MrpL55 protein is essential in *Drosophila* and dynamically required during development. *Exp Cell Res* 307: 354–366
- Vilkki J, Portin P (1987) Fine structure of flight muscles in different notch mutants of *Drosophila melanogaster* reared at different temperatures. *Roux Arch Dev Biol* 196: 12–15
- Wang ZA, Huang J, Kalderon D (2012) *Drosophila* follicle stem cells are regulated by proliferation and niche adhesion as well as mitochondria and ROS. *Nat Commun* 3: 769
- Wilson JJ, Kovall RA (2006) Crystal structure of the CSL-notch-mastermind ternary complex bound to DNA. *Cell* 124: 985–996
- Xu J, Chi F, Guo T, Punj V, Lee WN, French SW, Tsukamoto H (2015) NOTCH reprograms mitochondrial metabolism for proinflammatory macrophage activation. *J Clin Invest* 125: 1579–1590
- Yang SA, Deng WM (2018) Serrate/notch signaling regulates the size of the progenitor cell pool in *Drosophila* imaginal rings. *Genetics* 209: 829–843
- Yang L, Paul S, Trieu KG, Dent LG, Froidl F, Forés M, Webster K, Siegfried KR, Kondo S, Harvey K et al (2016) Minibrain and wings apart control organ growth and tissue patterning through down-regulation of Capicua. *Proc Natl Acad Sci USA* 113: 10583–10588
- Yu Z, Wu H, Chen H, Wang R, Liang X, Liu J, Li C, Deng WM, Jiao R (2013) CAF-1 promotes notch signaling through epigenetic control of target gene expression during *Drosophila* development. *Development* 140: 3635–3644
- Yuan Z, Praxenthaler H, Tabaja N, Torella R, Preiss A, Maier D, Kovall RA (2016) Structure and function of the Su(H)-hairless repressor complex, the major antagonist of notch signaling in *Drosophila melanogaster*. *PLoS Biol* 14: e1002509
- Zhang X, Gao X, Coots RA, Conn CS, Liu B, Qian SB (2015) Translational control of the cytosolic stress response by mitochondrial ribosomal protein L18. *Nat Struct Mol Biol* 22: 404–410
- Zhao L, Borikova AL, Ben-Yair R, Guner-Ataman B, MacRae CA, Lee RT, Burns CG, Burns CE (2014) Notch signaling regulates cardiomyocyte proliferation during zebrafish heart regeneration. *Proc Natl Acad Sci USA* 111: 1403–1408
- Zhao L, Gao F, Gao S, Liang Y, Long H, Lv Z, Su Y, Ye N, Zhang L, Zhao C et al (2021) Biodiversity-based development and evolution: the emerging research systems in model and non-model organisms. *Sci China Life Sci* 64: 1236–1280
- Zhao H, Ren X, Kong R, Shi L, Li Z, Wang R, Ma R, Zhao H, Liu F, Chang HC et al (2022) Auxilin regulates intestinal stem cell proliferation through EGFR. *Stem Cell Rep* 17: 1120–1137
- Zhou XL, Wu X, Xu QR, Zhu RR, Xu H, Li YY, Liu S, Huang H, Xu X, Wan L et al (2019) Notch1 provides myocardial protection by improving mitochondrial quality control. *J Cell Physiol* 234: 11835–11841

Expanded View Figures

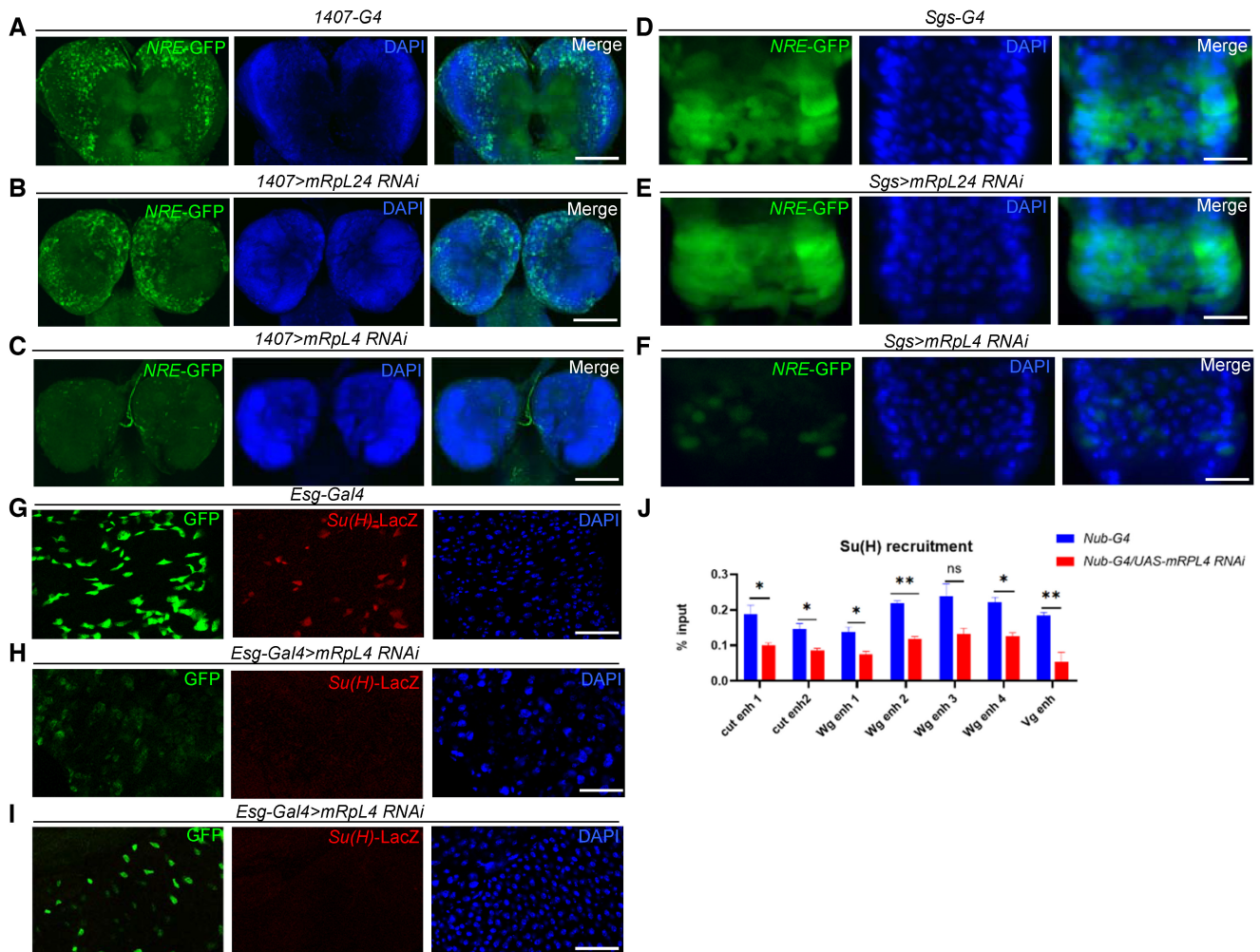


Figure EV1. Effects of mRpl4 RNAi on Notch signal activity.

A–C Representative image showing the expression of *NRE-GFP* in larval neuroblasts ($n > 10$ larvae) of control (A), mRpl24 RNAi (B) and mRpl4 RNAi (C) larvae.

D–F Representative image showing the expression of *NRE-GFP* in salivary gland imaginal rings ($n > 10$ larvae) of control (D), mRpl24 RNAi (E) and mRpl4 RNAi (F) larvae.

G–I Representative image showing the expression of *Su(H)-LacZ* in midgut cells ($n > 10$ flies) of control (G) and mRpl4 RNAi (H, I) adult flies.

J The level of *Su(H)* occupancy at *Wg*, *Cut* and *Vg* genomic regions as assessed by qPCR following ChIP, from wild-type and *UAS-mRpl4-RNAi*-expressing wing disks. Data are presented as mean \pm SEM, two biological replicates for each genotype and three technical replicates for each sample. Statistical significance was tested using two-tailed unpaired t-test. * $P < 0.05$, ** $P < 0.01$, ns means “not significant”.

Data information: Scale bars = 100 μ m.

Figure EV2. Effects of overexpressing Notch signaling components.

A–D Representative image of wing imaginal disks ($n > 10$ wing disks) containing MARCM clones stained for *Wg*. Notch signaling ligand *Dl* is overexpressed in wild-type (A) or *mRpl4*^{K14608} mutant (B) cells. Notch signaling ligand *Ser* is overexpressed in wild-type (C) or *mRpl4*^{K14608} mutant (D) cells.

E–H Representative image of wing imaginal disks ($n > 10$ wing disks) containing MARCM clones stained for NICD. Full-length Notch protein (*N^{F1}*) (E), NEXT (F) and NICD (G) are overexpressed in *mRpl4*^{K14608} mutant cells. Blank MARCM clones are generated in the wild-type wing disks (H).

Data information: The MARCM clones are marked by GFP and representative clones are marked by white arrows. Scale bars = 100 μ m.

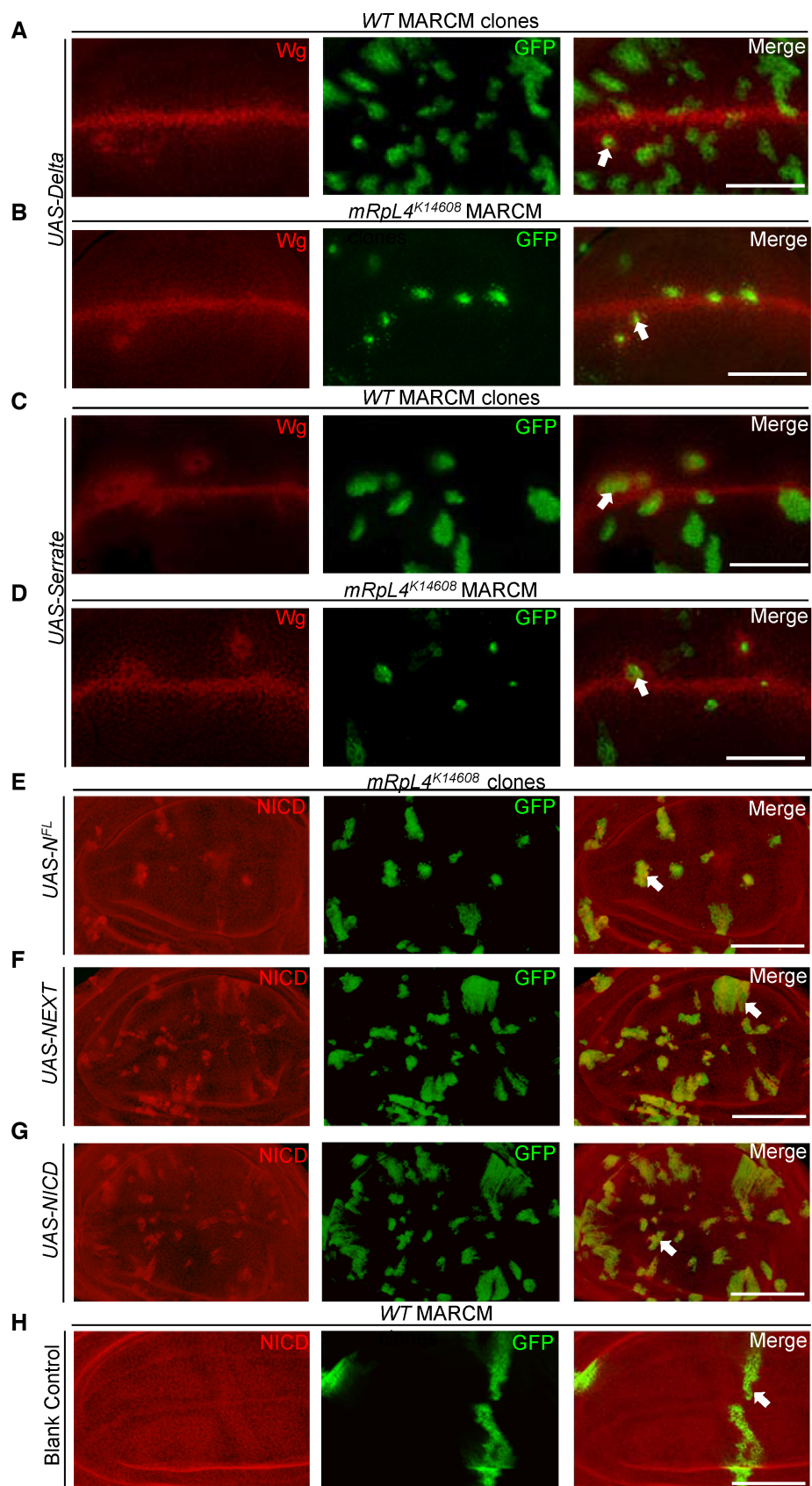


Figure EV2.

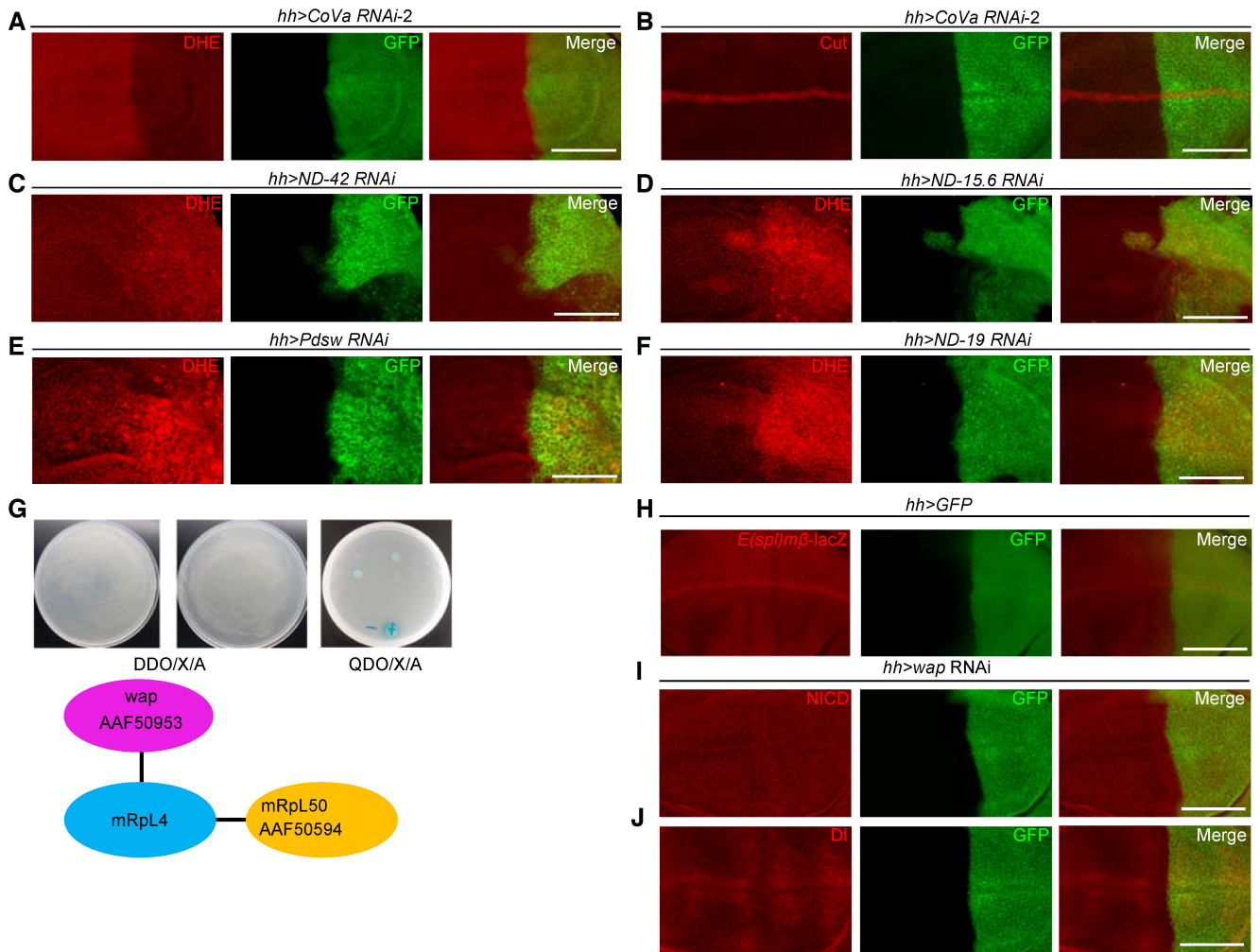


Figure EV3. mRpl4 may regulate OXPPOS activity and Notch signaling through branched pathways.

- A, B Representative images of wing imaginal disks ($n > 15$ wing disks) expressing *CoVa* RNAi under the control of *hh-gal4* (marked by GFP) that are stained for DHE (A) and Cut (B).
- C–F Representative images of wing imaginal disks ($n > 20$ wing disks) stained by DHE. The expression of *ND-42* (C), *ND-15.6* (D), *Pds* (E) and *ND-19* (F) RNAi are under the control of *hh-Gal4* (marked by GFP).
- G Two proteins, mRpl50 and wap are isolated as mRpl4 interaction partners through yeast two-hybridization. The GenBank accession numbers assigned to mRpl50 and wap are AAF50594 and AAF50953.
- H Representative image of wing imaginal disks ($n > 15$ wing disks) showing *E(spl)mβ-LacZ* expression pattern, and cells in the posterior compartment are marked by GFP.
- I, J Representative image of wing imaginal disks ($n > 15$ wing disks) stained for NICD (I) and DI (J). In these wing disks, *wap* RNAi are expressed under the control of *hh-Gal4* (marked by GFP).

Data information: Scale bars = 100 μ m.

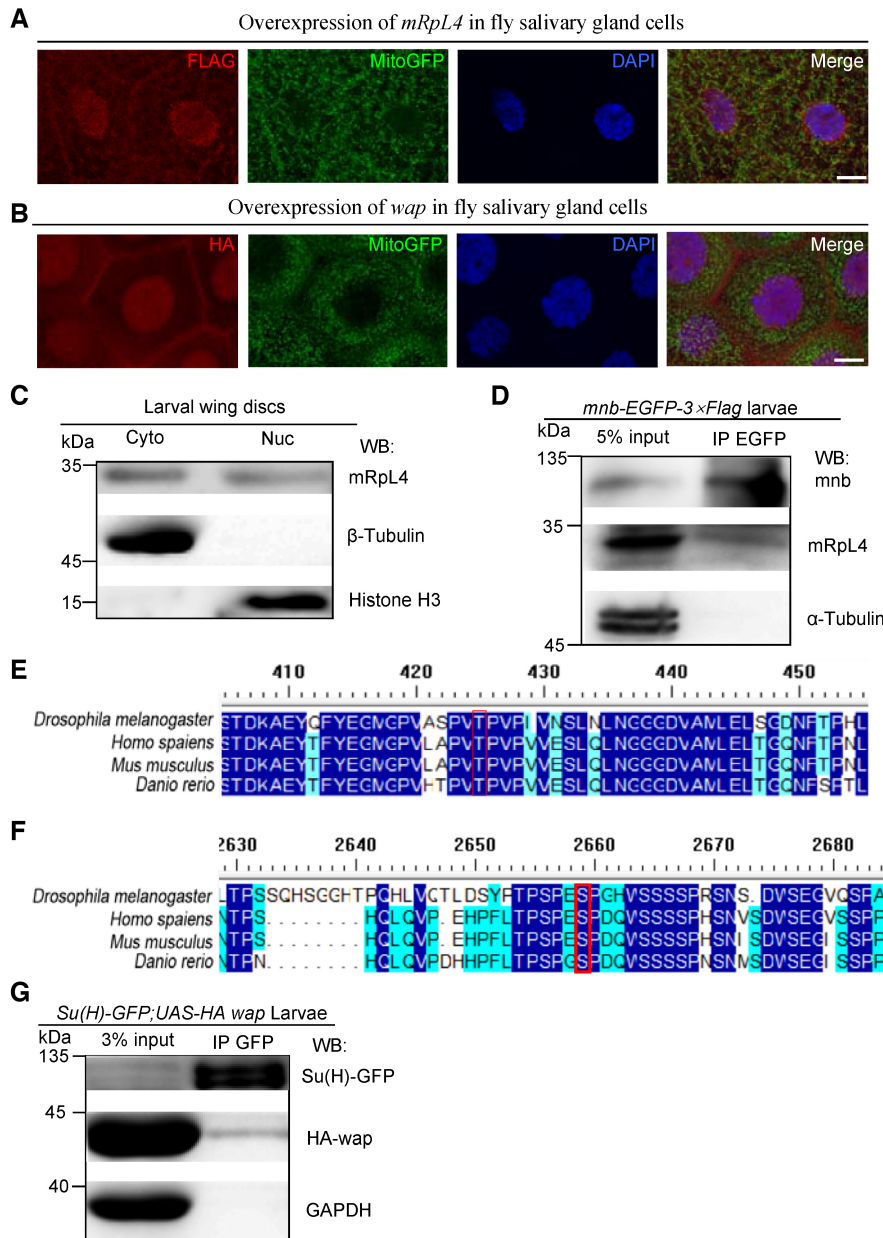


Figure EV4. mRpL4 and wap may function through Su(H) to regulate Notch signaling.

A, B Representative images of third instar larvae salivary glands ($n > 10$ larvae) from flies expressing FLAG-tagged mRpL4 (A) and HA-tagged wap (B). Immunostaining was performed using anti-FLAG and anti-HA antibodies to reveal mRpL4 and wap, respectively. Mitochondria are marked by GFP and cell nuclei are labeled by DAPI.

C Representative western blotting ($n = 3$ biological replicates) of mRpL4 protein distribution in cytoplasmic (Cyto) and nuclear (Nuc) fractions from wing discs lysates.

D Representative immunoprecipitation analysis ($n = 3$ biological replicates) using lysates from wing discs expressing GFP-tagged mnb. Anti-GFP antibodies were used for immunoprecipitation. Western blotting was performed using anti-GFP and anti-mRpL4 antibodies to reveal mnb and mRpL4, respectively. α-Tubulin was used as control.

E Alignment of Su(H) protein sequences from fly, human, mice and zebrafish. The region covering the mnb phosphorylation consensus sequence is shown, and the conserved Thr residue (T426) is labeled by red box.

F Alignment of Notch protein sequences from fly, human, mice and zebrafish. The region covering the mnb phosphorylation consensus sequence is shown, and the conserved Ser residue (S2659) is labeled by red box.

G Representative immunoprecipitation analysis ($n = 2$ biological replicates) using lysates from wing discs expressing GFP-tagged Su(H) and HA-tagged wap. Anti-GFP antibodies were used for immunoprecipitation. Western blotting was performed using anti-GFP and anti-HA antibodies to reveal Su(H) and wap, respectively. GAPDH was used as control.

Data information: Scale bars = 50 μm in (A and B). Source data are available online for this figure.

Appendix: Mo et al

Table of contents:

Appendix Table S1	2-3
Appendix Figure S1	4-5
Appendix Figure S2	6-7

Appendix Table S1: Sequences of primers used in this study

Primers for cDNA cloning

Target	Sequence (5' - 3')
<i>mRpL4</i> Forward	ATGTTGAACAATATTTTAAA
<i>mRpL4</i> Reverse	CTAGACTTGATCCAGCTTAA
<i>wap</i> Forward (HA tag)	ATGtacccttacgttctgattacgctagcctcTCCTCGAC CGCCGGAAA
<i>wap</i> Reverse	TTAGACCCGCAGGATCTC
<i>human-mRpL4</i> Forward	ATGCTGCAGTTCGTCCGGGC
<i>human-mRpL4</i> Reverse	CTAACAGCGGAGCCTGCACA
<i>zebrafish-mRpL4</i> Forward	CGCTATCACGACCTTCCTGAC
<i>zebrafish-mRpL4</i> Reverse	CCACTGAAGTCCATGCTGTTC
<i>zebrafish-hey1</i> Forward	GGATACGCGCTGCTAAACTGTC
<i>zebrafish-hey1</i> Reverse	TGGGACAAGCACAGTCGTTC

Primers for ChIP qPCR

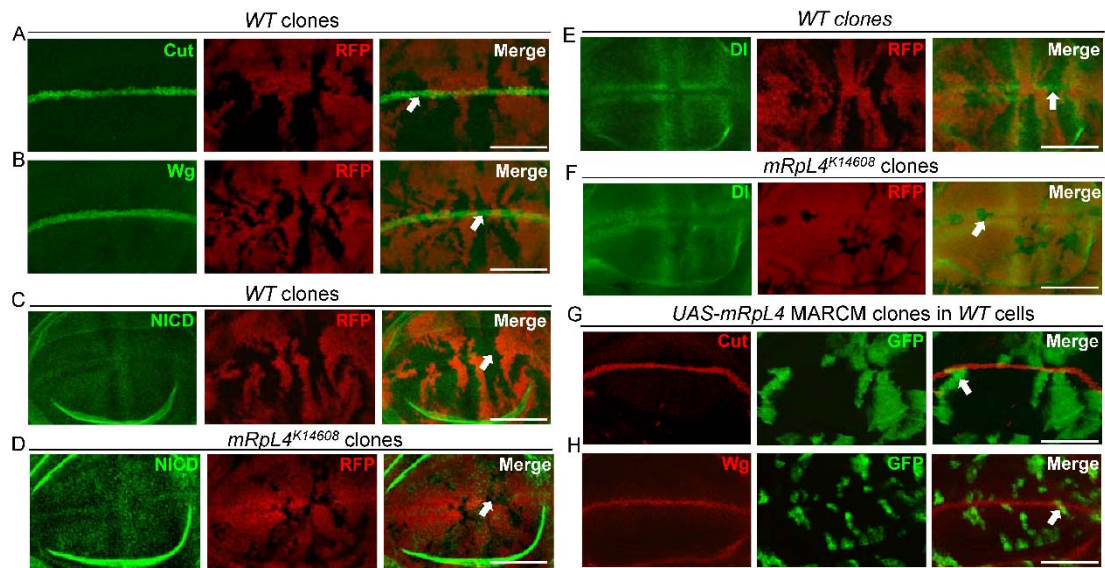
Target	Sequence (5' - 3')
<i>mγ-mβ igr</i> Forward	GGAGTTGAGGAGTTGGTCG
<i>mγ-mβ igr</i> Reverse	ATAAGTGTGGTTGGGTGCCT
<i>mβ-tr</i> Forward	AGAAGTGAGCAGCAGCCATC
<i>mβ-tr</i> Reverse	GCTGGACTTGAAACCGCACC
<i>mβ-enh</i> Forward	AGAGGTCTGTGCGACTTGG
<i>mβ-enh</i> Reverse	GGATGGAAGGCATGTGCT
<i>mβ-mα igr</i> Forward	AAGCCAGTGGACTCTGCTCT
<i>mβ-mα igr</i> Reverse	TGATCTCCAAGCGGAGTATG
<i>mα-tr</i> Forward	GCAGGAGGACGAGGAGGATG
<i>mα-tr</i> Reverse	GATCCTGGAATTGCATGGAG
<i>m2-m3 igr</i> Forward	GCGCGTATTTCCCAAATAAA
<i>m2-m3 igr</i> Reverse	GATTGTACGTGCATGGGAAA
<i>m3-enh</i> Forward	ACACACACAAACCCCATCC
<i>m3-enh</i> Reverse	CGAGGCAGTAGCCTATGTGA
<i>m3-tr</i> Forward	CGTCTGCAGCTCAATTAGTC
<i>m3-tr</i> Reverse	AGCCCACCCACCTCAACCAG
<i>Cut enh Forward1</i>	CCGATAAATCGGGGTTTTGGA
<i>Cut enh Reverse1</i>	ACGCCTGTTACCATAGTCGC
<i>Cut enh Forward2</i>	TTTGCCGACGTGAGAAACAC
<i>Cut enh Reverse2</i>	TCCTCCTTTTTCATACTTCATTAC
<i>Wg enh Forward1</i>	CCGTACTTTTTCCGGACCAC
<i>Wg enh Reverse1</i>	CGCTAAGCCCCTGTTTGGT
<i>Wg enh Forward2</i>	TGCTCCTCTGACCACGATCC

<i>Wg enh Reverse2</i>	CCTTAAGCCGCCTCGACTG
<i>Wg enh Forward3</i>	CGCCGAAACATTTTCGAGAAACA
<i>Wg enh Reverse3</i>	CGTGACGCACAAGACCTTTA
<i>Wg enh Forward4</i>	GCATTGCGCAACGTTTCGGT
<i>Wg enh Reverse4</i>	AAATGTTTATTGACAGGCAGCGG
<i>Vg enh Forward1</i>	CCTCTCCCGCTTTTTGCTAAC
<i>Vg enh Reverse1</i>	ACTGGACACTGGAAACCAGC

Primers for RT-qPCR assay

Target	Sequence (5' - 3')
<i>zebrafish-mRpL4</i> Forward	TCAGATCTTCCAGTTGTGCG
<i>zebrafish-mRpL4</i> Reverse	GTTTGAAGTTCCGTTGCCAG
<i>zebrafish-notch1a</i> Forward	CGACACCACACACACATGCT
<i>zebrafish-notch1a</i> Reverse	AGTGGCAGTTGTAGGTGTTG
<i>zebrafish-hey1</i> Forward	GCCTTTGAGAAACAGGGCTCAG
<i>zebrafish-hey1</i> Reverse	AGCGTGAGCATCAAAGTAACCT
<i>zebrafish-her4.1</i> Forward	AGGAGAACTGAACACAAGACAC
<i>zebrafish-her4.1</i> Reverse	TGCTGTTGATTCGCTCTCG
<i>zebrafish-her6</i> Forward	GGCTTCGGAACACAGAAAG
<i>zebrafish-her6</i> Reverse	TGACCCAAGCTTTCGTTGA
<i>zebrafish-her15.1</i> Forward	TCGCTCTGCTCAGAGAAACA
<i>zebrafish-her15.1</i> Reverse	ACCACTGGCTTTCGCAA
<i>zebrafish-β-actin</i> Forward	ATCTTCACTCCCCTTGTTTAC
<i>zebrafish-β-actin</i> Reverse	TCATCTCCAGCAAAAACCGG

Appendix Figure S1. Expression pattern of Notch signaling components.



A Representative images of wing imaginal disc ($n > 10$ wing discs) bearing wild type clones stained for Cut.

B Representative images of wing imaginal disc ($n > 10$ wing discs) bearing wild type clones stained for Wg.

C Representative images of wing imaginal disc ($n > 10$ wing discs) bearing wild type clones stained for NICD.

D Representative images of wing imaginal disc ($n > 15$ wing discs) bearing *mRpL4^{K14608}* clones stained for NICD.

E Representative images of wing imaginal disc ($n > 15$ wing discs) bearing wild type clones stained for Dll.

F Representative images of wing imaginal disc ($n > 15$ wing discs) bearing *mRpL4^{K14608}* clones stained for Dll.

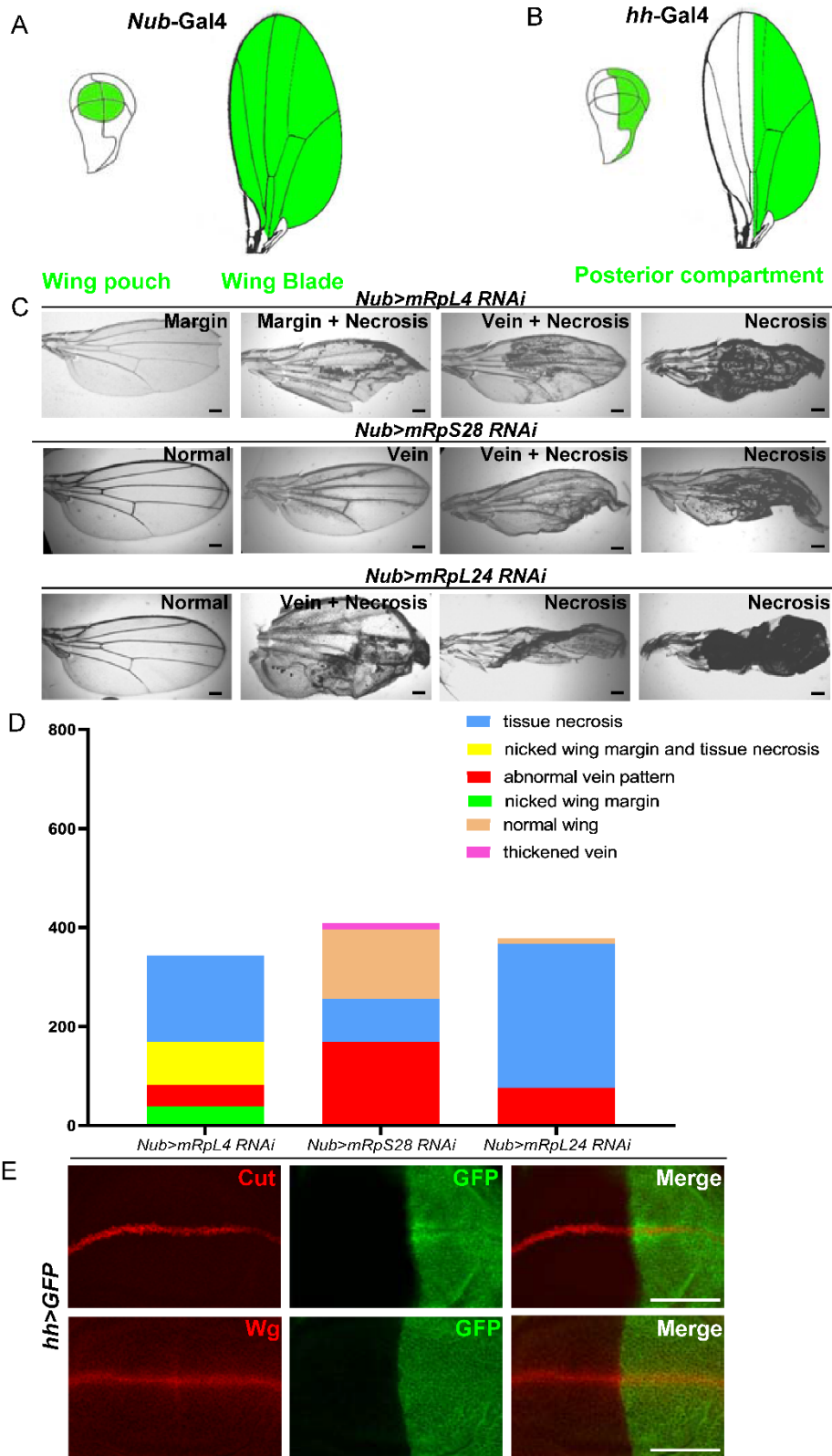
G Representative images of wild type wing imaginal disc ($n > 10$ wing discs) bearing *UAS-mRpL4* MARCM clones stained for Cut.

H Representative images of wild type wing imaginal disc ($n > 10$ wing discs) bearing

UAS-mRpL4 MARCM clones stained for Wg.

Data information: Clones are marked by absence of RFP (*A-F*), while the MARCM clones are marked by GFP (*G* and *H*). Representative clones are marked by white arrows. Scale bars = 100 μm .

Appendix Figure S2. Effects of MRPs knock-down.



A, B Cartoons showing the areas where *Nub-Gal4* (*A*) and *hh-Gal4* (*B*) are active.

C Representative images of adult wings ($n > 15$ wings) showing diverse defects upon

knock-down of *mRpL4*, *mRpS28* and *mRpL24* by *Nub*-Gal4 driven RNAi.

D Quantification of adult wing defects. mRpL4 RNAi led to wing margin nicks in 11.08% of the wings, and wing margin nicks along with tissue necrosis in 25.66% of the wings (n = 343). After knock-down mRpS28 (n = 408) or mRpL24 (n = 378) by RNAi, wing margin nicking defects were not observed.

E Representative images of wing imaginal disc ($n > 15$ wing discs) expressing GFP under the control of *hh*-Gal4 stained for Cut and Wg.

Data information: Scale bars = 100 μ m.